Morphological and Multivariate Statistical Analysis of Quaternary Monogenetic Vents in the Central Anatolian Volcanic Province (Turkey): Implications for the Volcano-Tectonic Evolution

Göksu Uslular[a,b], Nicolas Le Corvec[c], Francesco Mazzarini[d], Denis Legrand[e], Gonca Gençalioğlu-Kuşcu[a]

Corresponding author: goksuuslular@mu.edu.tr; goeksu.uslular@etu.unige.ch

[a]*Department of Geological Engineering, Muğla Sıtkı Koçman University, Kötekli Campus, Muğla, 48000TR, Turkey*
[b]*Department of Earth Sciences, University of Geneva, Geneva 1205, Switzerland*
[c]*Laboratoire Magmas et Volcans, Université Clermont Auvergne–CNRS–IRD, OPGC, Aubière, France*
[d]*Istituto Nazionale di Geofisica e Vulcanologia (INGV), Via Cesare Battisti, 53, 56125 PISA Italy*
[e]*Universidad Nacional Autonoma de Mexico (UNAM), Mexico City, Mexico*

Abstract

The interaction and competition between magmatic and tectonic processes mostly control the spatial distribution and morphology of monogenetic volcanoes. The Central Anatolian Volcanic Province (CAVP) situated in a strike-slip environment provides a remarkable opportunity to understand this relation. In this study, we defined six monogenetic volcanic fields within the CAVP and analyzed a total number of 540 monogenetic volcanoes in terms of morphological and spatial characteristics. The morphological characteristics favour the dominant role of magmatic eruptions over the phreatomagmatic ones supported by the types of monogenetic volcanoes. The flank slopes are probably the best morphometric parameters that display a correlation with the ages, and hence its usage in the relative-dating studies might be promoted. The spatial distribution of the vents in the CAVP shows a self-similar (fractal) clustering that obeys the power-law distribution defined over a range of lower (L_{co}) and upper (U_{co}) cut-off distances. The computed fractal dimensions (D_f) of the six monogenetic volcanic fields vary in the range of 1.16 to 1.80, possibly due to the slight variation in the crustal thickness and fracture distribution. U_{co} values interpreted as the initial depth of dike intrusions are well-correlated with the local tectonics and vary from north (8.5 to 12 km) to south (16 km).

Both clustered and non-clustered vent distributions are observed in the CAVP according to the Poisson nearest neighbor analysis. The former case indicates the vents formed by a single centralized plumbing system (e.g. Erciyes volcanic complex "EVC"), while the latter refers to the formation of vents through the independent shallow or deep magma reservoirs (e.g. Acıgöl volcanic complex). The pre-existing fractures and the changes in the local and regional stress fields are the prevalent mechanisms for the emplacement and the spatial distribution of vents. The EVC having formed along the Central Anatolian Fault Zone (CAFZ) is here considered as a magmatic transfer zone mostly inferred from the presence of many strike-slip features, rotation of extension axis, and the radial pattern of the vents. Through the western parts of CAVP, the vent alignments are almost perpendicular to the regional extension axis and parallel to the orientation of the Tuz Gölü Fault Zone (TGFZ) where the pre-existing fractures are probably the primary mechanisms on their formations.

Our comprehensive approach together with the analysis of well-established literature reveals that the collision along the Bitlis suture zone in the middle Miocene and subsequent westward tectonic escape of the Anatolia along the major fault zones have mostly controlled the volcanism not only in eastern Anatolia but also in the CAVP. In this scenario, we suggest that the CAFZ has been the main mechanism for the propagation of mantle-derived magmas and completely shaped the spatial distribution of the volcanoes in the CAVP with the help of crustal-depth TGFZ and other tectonic features. Our recent findings presented here will hopefully offer new insights into the understanding of CAVP volcanism and the intended future volcanic risk assessment studies.

Keywords: Self-Similar Clustering, Vent Alignment, Strike-Slip Tectonism, Monogenetic Volcanism, Cenral Anatolian Volcanic Province

1. Introduction

Monogenetic volcanic fields (hereafter MVFs) are the most common volcanic landforms on Earth and can be found in all tectonic settings but mostly in extensional environments (e.g. Le Corvec et al., 2013a). Monogenetic edifices are small volume volcanoes (< 1 km^3) formed by one continuous or many discontinuous small dry and/or wet eruptions (Németh and Kereszturi, 2015). Surface morphology affected by internal (e.g. magma rheology, rate of ascent, and magma/water ratio) and external (e.g. tectonic features, climate) factors reveals various types including scoria cones, maars (maar-diatremes), spatter cones, lava domes, tuff cones and tuff rings (Németh, 2010; Kereszturi and Németh, 2012a; Németh and Kereszturi, 2015; Németh and Kósik, 2020). Scoria cones and maars, which are generally mafic to intermediate in composition, are the most common monogenetic edifices (Lorenz, 1975; Settle, 1979). MVFs consist of tens to several hundreds of volcanic centers that create either their own fields (e.g. Michoacan-Guanajuato Volcanic Field, Mexico, Connor, 1987) or are located at the flanks of composite volcanoes (e.g. Mauna Kea Volcano, Porter, 1972; Mount Etna Volcano, Mazzarini and Armienti, 2001). The spatial distribution of vents in the MVFs has been analyzed by different methods (e.g. self-similar clustering, vent alignment analysis) for several decades to understand the link between tectonism and magmatism (Connor, 1987; Le Corvec et al., 2013a; Muirhead et al., 2015; Haag et al., 2019; Murcia et al., 2019; Cañón-Tapia, 2020). As each volcanic center represents the last point of magma pathway en-route to the surface either from the shallow (e.g. lava domes) or deep (e.g. scoria cones) magma reservoirs, the alignment and/or clustering of these vents in the MVFs are the possible surface expressions of the magma plumbing systems especially in the brittle upper crust (e.g. Brenna et al., 2011; Germa et al., 2013; Le Corvec et al., 2013a; Muirhead et al., 2015).

The morphological analysis of monogenetic volcanoes (mostly scoria cones) also provides new insights into the understanding of both internal and external factors in their formation (Wood, 1980; Riedel et al., 2003; Dóniz et al., 2008; Favalli et al., 2009; Rodriguez-Gonzalez et al., 2010; Inbar et al., 2011; Kereszturi et al., 2012; Kervyn et al., 2012; Bemis and Ferencz, 2017). The morphometry-based studies mostly tackled the reasons for various sizes and shape, and the factors (e.g. magma rheology, degradation processes, climate) responsible for these morphometric differences in monogenetic volcanoes. Most of the interpretations related to morphology have been generally considered as indirectly contributing to the tectonomagmatic evolution of MVFs, but the role of fault geometry in the eruptive dynamics and morphology has been recently revealed (Gómez-Vasconcelos et al., 2020). There are also many attempts to explore the possible link between the temporal evolution of MVFs and the morphology (i.e. relative dating of scoria cones) and also a few more suggesting the fractal behaviour of size-distribution (i.e. width of scoria cones, Kurokawal et al. 1995; Pérez-López et al., 2011; Uslular et al., 2015). Consequently, the conflation of the various approaches mentioned above for a better understanding of the whole evolutionary mechanisms in the MVFs does certainly provide new insight into the possible link between tectonism and volcanism.

In this study, we performed morphological, statistical (self-similar clustering, principal component, vent-to-vent distance, Poisson nearest neighbour), and vent alignment analyses on Quaternary monogenetic vents in the Central Anatolian Volcanic Province (CAVP), one of the most spectacular volcanic fields in Anatolia with various types of Miocene-Quaternary polygenetic and several hundreds of Quaternary monogenetic volcanoes (Toprak, 1998) (Fig. 1). We revised the comprehensive database of Arcasoy (2001) by selecting the most representative Quaternary monogenetic vents (540) and classified them based on their types (i.e. scoria cone, lava dome and maar). Here, we focused especially on the scoria cones and lava domes to define their morphological characteristics and to create a link between their spatial distributions and the tectonism in the CAVP. Our approach presented in this study will certainly contribute to the understanding of the well-known role of tectonism on the widespread volcanism in the CAVP (e.g. Pasquare et al., 1988; Göncüoğlu and Toprak, 1992; Toprak and Göncüoglu, 1993; Dhont et al., 1998; Toprak, 1998) by providing new insight into the mechanical behaviour of the crust beneath the region.

2. Quaternary Monogenetic Clusters in the CAVP

Central Anatolia is a high plateau (~ 1 km a.s.l; Çiner et al., 2015) within a relatively small region (300 x 400 km) located at the Kırşehir block between Pontide and Anatolide-Tauride orogenic mountain belts (e.g. Okay and Tüysüz, 1999) (Fig. 1A). Volcanism has initiated in the late Cretaceous within the Sakarya zone (NW of Kırşehir block; Galatia volcanics; *ca.* 76 Ma, Koçyiğit and Beyhan, 1998) during the almost coeval closure of the northern Neo-Tethys ocean along the İzmir-Ankara-Erzincan suture zone (e.g. Okay and Tüysüz, 1999; Pourteau et al., 2013) (Fig. 1A). After the initiation of a collision between Arabian and Eurasian plates along the Bitlis suture zone that resulted in the closure of the southern Neo-Tethys during the middle Miocene (Okay et al., 2010; Cavazza et al., 2018), the volcanism has continued in the Galatia (*ca.* 19 Ma to Pliocene?; Wilson et al., 1997) and spread throughout the approximate borders of Kırşehir block (Karacadağ to the west, *ca.* 21-14 Ma, Asan and Kurt, 2011; Erenlerdağ-Alacadağ-Sulutaş to the southwest, *ca.* 22-3 Ma, e.g. Gençoğlu-Korkmaz et al., 2017; Sivas to the east, *ca.* 23-4 Ma, e.g. Kocaarslan and Ersoy, 2018; Reid et al., 2019). The CAVP within this realm is located at the southern part of Kırşehir block and extending through the Anatolide-Tauride platform as a NE-SW trending volcanic belt bounded by two major transcurrent faults, Tuz Gölü Fault Zone (TGFZ) and Central Anatolian Fault Zone (CAFZ) with its southern component Ecemiş fault (Toprak and Göncüoglu, 1993; Koçyiğit and Beyhan, 1998; Çemen et al., 1999; Koçyiğit and Erol, 2001) (Fig. 1B). The extensional tectonic regime in the CAVP has been possibly active since late Miocene (e.g. Göncüoğlu and Toprak, 1992; Dhont et al., 1998; Özsayın et al., 2013). The NNW-SSE to NE-SW compressional stress regime tailed off in the late Miocene (e.g. Özsayın et al., 2013), and subsequently, the extensional regime along with the N-S to NE-SW trending has been active during the Pliocene-Quaternary period (Göncüoğlu and Toprak, 1992). The widespread volcanism initiated during the middle Miocene and continued to the Holocene times hinged on the available geochronology data (13.7 $\pm$ 0.3 Ma, K-Ar, Keçikalesi caldera, Besang et al., 1977; 8.97 $\pm$ 0.64 ka, (U-Th)/He, 2σ, Hasandağ strato-volcano, Schmitt et al., 2014; Fig. 1B). There are also some recent attempts to explore this relatively complex geodynamic setting and its role in the evolution of widespread CAVP volcanism (Bartol and Govers, 2014; Delph et al., 2017; Göğüş et al., 2017; Reid et al., 2017; Di Giuseppe et al., 2018; Rabayrol et al., 2019). Although details of these geodynamic models are beyond the scope of this study, we are here required to briefly explain them for a better understanding of the evolutionary processes, especially in the Quaternary period. Roll-back of the Cyprus slab since early (e.g. Biryol et al., 2011; Rabayrol et al., 2019) or middle (Abgarmi et al., 2017) Miocene resulted in the delamination (Bartol and Govers, 2014; Delph et al., 2017) or dripping (Göğüş et al., 2017) of the sub-continental lithospheric mantle (SCLM). This has been considered as the initiation of the CAVP volcanism (especially ignimbrite flare-ups; e.g. Aydar et al., 2012) pertaining to the uprising asthenosphere (e.g. Delph et al., 2017). Subsequent break-off of the subducting African lithosphere, which is coeval with the uplift of the central Anatolia (*ca.* 8 Ma; Cosentino et al., 2012; Schildgen et al., 2014) and leads to the upwelling of asthenosphere through the gap, has been mainly linked with the late Miocene to recent volcanism in the CAVP (Abgarmi et al., 2017; Delph et al., 2017; Reid et al., 2017; Schleiffarth et al., 2018). However, there are some interrogable parts in the evolutionary models, e.g. temporally scattered pattern of volcanism (at least within the CAVP, cf. Schleiffarth et al., 2018; Rabayrol et al., 2019); the presence of alternative mechanisms for thin SCLM, regional uplift and even upwelling asthenosphere in the post-collisional settings (e.g. Gençalioğlu-Kuşcu and Geneli, 2010; Kaislaniemi et al., 2014); and also the existence of heterogeneous mantle source composed of dominantly metasomatized SCLM with a limited contribution of almost geochemically unrevealable asthenosphere (Uslular and Gençalioğlu-Kuşcu, 2019b). Alternatively, with some more critics on the available models, Rabayrol et al. (2019) proposed a new and disputable model involving the slab-tearing (Arabian segment) and partial SCLM removal during the last 16.5 Ma as a possible mechanism for the widespread volcanism in both central and eastern Anatolia. In summary, the CAVP within an extensional tectonic regime has been currently sitting on a *ca.* 35-40 km thick crust including low seismic velocity layers ranging from 15 to 25 km depth (possible crustal magma reservoirs; Abgarmi et al., 2017) that overlies the relatively thin metasomatized SCLM and an underlying hot asthenosphere.

The CAVP exhibits many spectacular volcanic landscapes including Miocene-Pliocene widespread ignimbrites with well-preserved fairy-chimneys (e.g. Aydar et al., 2012; Çiner and Aydar, 2019), various types of Miocene-Quaternary polygenetic volcanoes (e.g. Hasandağ and Erciyes stratovolcanoes, Keçikalesi and Acıgöl calderas) and numerous (> 800) Quaternary monogenetic volcanoes (dominantly scoria cones with subordinate domes and a few maars and tuff rings) (Toprak, 1998; Arcasoy, 2001; Arcasoy et al., 2004). Monogenetic volcanoes in the CAVP, as the main subject of this study, are formed either on the flanks of polygenetic volcanoes (e.g. Erciyes stratovolcano) or as a resurgent phase in calderas (e.g. Acıgöl and Derinkuyu calderas), or in their own MVFs (Eğrikuyu and Karapınar monogenetic fields) (Toprak, 1998; Uslular et al., 2015; Uslular and Gençalioğlu-Kuşcu, 2019b) (Fig. 1B). They are mainly clustered in six distinct regions (Fig. 1B) based on the spatial distributions of vents and also volcanological evolution of the adjacent field (slightly modified after Toprak, 1998). In the following section, we give some introductory information about the volcanological evolution of these MVFs in the light of well-established literature.

2.1. Erciyes Volcanic Complex (EVC)

The volcanological evolution of EVC is represented by two successive stratovolcano formations (Şen, 1997; Şen et al., 2003) (Figs. 1B and 2). Koçdağ stratovolcano represents the older stage consisting of lava flows and pyroclastics related to initial scoria cone-forming eruptions, and pyroclastic fall and flow deposits formed by the latter calderaforming eruptions (Şen et al., 2003). Of these, Valibaba Tepe ignimbrite (2.52 ± 0.49 Ma; Aydar et al., 2012) with a volume of 40 km^3 is considered as the last product of the Koçdağ stage (Şen et al., 2003). However, a scoria cone (Kızıltepe) that belongs to the older phase of Koçdağ stage has been recently dated as 0.71 ± 0.02 Ma (Doğan-Külahçı et al., 2018), and hence there is a need for reconsideration of the temporal evolution of this stage. Mount Erciyes (*Argus* in Latin, firstly mentioned in Strabo's book of 'Geographica', Hamilton and Falconer, 1903) is a spectacular Quaternary stratovolcano formed in a pull-apart basin and represents the last stage of EVC (Şen, 1997; Toprak, 1998; Şen et al., 2003; Aydar et al., 2019) (Figs. 1B and 2). Erciyes stage is characterized by two eruptive cycles: in one, andesitic-dacitic lava domes and basaltic andesitic scoria cones with related lava flows (also a maar, namely Cora; Gençalioğlu-Kuşcu et al., 2007) emanated from effusive-explosive eruptions formed the main volcano edifice, whereas, in the other, more dominant explosive eruptions generated lava domes and related deposits at the summit of Erciyes stratovolcano (Şen et al., 2003). Most of the monogenetic volcanoes are located at the flanks of Erciyes stratovolcano with an almost radial spatial trend (dominantly NE-SW; Table 1). Although the significant number of vents are Pleistocene in age, there also some Holocene lava dome activity in the EVC (Şen et al., 2003; Sarıkaya et al., 2019; Friedrichs et al., 2020b). Some of the individual monogenetic volcanoes were investigated in terms of both volcanological and petrological characteristics. Dikkartın lava dome with a rhyodacitic composition is one of the most studied monogenetic volcanoes in the EVC, and its age (10.3 ± 0.5 ka, ^{36}Cl, Sarıkaya et al., 2019; 7.9 ± 0.5 ka, 1σ, (U-Th)/He, Friedrichs et al., 2020b), tephra dispersion (> 600 km away from its source towards the southeastern part of Mediterranean; Hamann et al., 2010) and depositional characteristics (Şen et al., 2002; Ersoy et al., 2019) are well established. In addition, Cora maar with a basaltic andesitic composition is the only well-preserved phreatomagmatic edifice in the EVC and displays almost all characteristic features of base-surge deposits observed in maar volcanoes (e.g. dunes, accretionary lapilli, cauliflower bombs; Gençalioğlu-Kuşcu et al., 2007; Gençalioğlu-Kuşcu, 2011). Moreover, Higgins et al. (2015) dated two aligned lava domes near Dikkartın (210 ± 18 ka and 580 ± 130 ka, 2σ, Ar-Ar) and also claimed that the most dominant trend of the vents especially those in the southwestern flank is N32°E based on the spatial analysis of vent distribution (parallel to the main trend of CAFZ; e.g. Koçyiğit and Beyhan, 1998), indicating a WNW-ESE extension along the

NNE trending Dündarlı-Erciyes fault (DEF, Fig.2).

2.2. *Nevşehir-Acıgöl Volcanic Complex (NAVC)*

Two distinct calderas (namely Nevşehir and Acıgöl) with related voluminous ignimbrites and numerous monogenetic volcanoes (mostly lava domes and scoria cones with a few maars and tuff rings) characterize the volcanological evolution of the NAVC (Aydar et al., 2011). Some of the older ignimbrite deposits in the CAVP are considered to emanate from a buried caldera corresponding to a depression within the NAVC (Aydar et al., 2012) (Figs. 1B and 2). This depression with a 15 km sub-circular shape is only detected by geophysical surveys (Froger et al., 1998; Ulusoy et al.; Aydar et al., 2011); nevertheless it is one of the most probable candidates for so-called "Nevşehir" caldera that is the source of these two older and widespread ignimbrite deposits supported by some stratigraphical and structural findings (e.g. Le Pennec et al., 1994; Froger et al., 1998). There are a few lava domes along the Derinkuyu fault (DF) that probably post-date the Nevşehir caldera (Figs. 1B and 2).

Acıgöl (or Kocadağ) caldera is located at the western part of buried Nevşehir caldera and involves the youngest ignimbrite deposits (namely Kumtepe, Aydar et al., 2012) and various monogenetic volcanoes in the CAVP (Yıldırım and Özgür, 1981; Druitt et al., 1995; Froger et al., 1998; Mouralis et al., 2002; Schmitt et al., 2011). Although still there is no consensus on the exact location and hence the boundaries of the caldera (e.g. Yıldırım and Özgür, 1981; Druitt et al., 1995; Froger et al., 1998), the preferred location and the shape (ellipsoidal with the dimensions of 8 x 12 km; Fig. 2) seem more promising (Yıldırım and Özgür, 1981). Kumtepe ignimbrite consists of two successive eruption units separated by paleosols and scoria fall deposits, namely the Lower and Upper Acıgöl Tuffs (LAT and UAT, respectively; Druitt et al., 1995; Aydar et al., 2011). The recently updated ages of these deposits are 190 $\pm$ 11 ka (LAT) and 164 $\pm$ 4 ka (UAT; 1σ; U-Th/He on zircon; Atıcı et al., 2019). The resurgent lava domes with dacitic to rhyolitic composition (e.g. Türkecan et al., 2004; Siebel et al., 2011) are the most abundant monogenetic edifices in Acıgöl caldera (Table 1), and they form two spatially distinct clusters: the first one consisting of older domes in the east (e.g. Kocadağ, 190 $\pm$ 26 ka; Taşkesik, 147 $\pm$ 18 ka; (U-Th)/He, 2σ, Schmitt et al., 2011), and the second one involving younger domes in the west (e.g. Kalecitepe, 23.2 $\pm$ 9.7 ka; Korudağ, 24.3 $\pm$ 2.1 ka; 2σ, Schmitt et al., 2011) (Fig. 2). Maars, tuff rings and explosion craters are the second common monogenetic volcanoes in the region (Table 1). They are mostly rhyolitic in composition, except the basaltic İcik maar and Karataş tuff ring (Aydar et al., 2011; Türkecan et al., 2004; Uslular and Gençalioğlu-Kuşcu, 2020) (Fig. 2). Of those, Acıgöl coalescence maar (20.3 ± 0.9 ka, 2σ, Schmitt et al., 2011) is the only studied one in terms of volcanological and paleoclimatological characteristics (Kazancı et al., 1995; Roberts et al., 2001; Mouralis et al., 2002; Tuncer et al., 2019; Uslular and Gençalioğlu-Kuşcu, 2020). Most other maars in the CAVP, such as Kalecitepe located at the northwestern part of Acıgöl maar complex, involve a lava dome in their center that postdates the maar formation (Schmitt et al., 2011; Uslular and Gençalioğlu-Kuşcu, 2020). Scoria cones of basaltic to andesitic compositions are more scarce within the NAVC, and their formation is mostly coeval with the other monogenetic edifices hinged on the available geochronology data (32-620 ka, K-Ar; Türkecan et al., 2004).

2.3. Derinkuyu Volcanic Complex (DVC)

The DVC is represented by a buried caldera complex (i.e. Derinkuyu, Froger et al., 1998) including resurgent dome complexes, numerous scoria cones, and a maar volcano (Narlıgöl, Gevrek and Kazancı, 2000) (Figs. 1B and 2). This caldera complex consists of at least four mostly buried calderas, which are only detected via some geophysical surveys and satellite data (Froger et al., 1998) and are the possible sources for several widespread ignimbrite deposits (i.e. Sarımaden, Cemilköy, Gördeles, and Kızılkaya; *ca.* 8.5-5.1 Ma; Le Pennec et al., 1994; Aydar et al., 2012). The resurgent Quaternary dome complexes (Şahinkalesi and Göllüdağ) in the southern part of the DVC (0.09-1.10 Ma; Türkecan et al., 2004; Aydin et al., 2014)(Figs. 1B and 2) were possibly located at the center of two temporarily successive buried calderas that had produced Gördeles and Kızılkaya ignimbrites (6.33 ± 0.23 Ma and 5.11 ± 0.37 Ma, respectively; Aydar et al., 2012) (Le Pennec et al., 1994; Froger et al., 1998). Another important rhyolitic dome within the DVC (namely Nenezi, 92 ± 4 ka, K-Ar; Türkecan et al., 2004) is just located at the northwestern part of the Şahinkalesi dome complex (Fig. 2). Scoria cones with basaltic to basaltic andesitic compositions (Türkecan et al., 2004; Aydin et al., 2014) are mainly concentrated in the northern parts between lava dome complexes to the south and the Erdaş stratovolcano (or Kızılçın; 11.1-8.4 Ma; Ar-Ar; Aydar et al., 2011) to the north

(Fig. 2). The available geochronology data on scoria cones (Türkecan et al., 2004; Aydin et al., 2014) proclaim that their formations are mostly coeval with those of lava domes in the NAVC. Narlıgöl is the only maar in the NAVC with a basaltic composition and lithic-rich pyroclastic deposits (Uslular and Gençalioğlu-Kuşcu, 2020) (Fig. 2). Also, the maar is geothermally active with hot springs (Gevrek and Kazancı, 2000), and when this is combined with the other implications such as hydrothermal activity (e.g. kaolinization in ignimbrites), gas emissions and other hot springs, it can be deduced that there would be still partially hot underlying magma reservoir in the DVC (e.g. Froger et al., 1998).

2.4. Hasandağ-Keçiboyduran Volcanic Complex (HKVC)

The HKVC consists of two stratovolcanoes (namely Hasandağ and Keçiboyduran) and related numerous monogenetic volcanoes (Figs. 1B and 2). The spatial distribution of monogenetic volcanoes around these major volcanoes was previously considered as different clusters (Toprak, 1998), but we here combined them as most of the Quaternary vents emanated from Keçiboyduran stratovolcano are mainly concentrated through the eastern flanks of Hasandağ stratovolcano (Fig. 1B). Also, the clusters of numerous scoria and spatter cones related to Keçiboyduran-Melendiz fault zone (Toprak and Göncüoglu, 1993) around the northern part of Keçiboyduran stratovolcano are evaluated within the HKVC cluster (Fig. 1B). The dextral Tuzgölü fault zone (TGFZ) and its components have a direct role in the formation of volcanism in and around the HKVC (e.g. Toprak and Göncüoglu, 1993; Dhont et al., 1998; Toprak, 1998). The alignment of monogenetic vents in the region with a dominant trend of NW-SE also clearly supports this claim (Toprak, 1998).

The volcanism in Hasandağ stratovolcano initiated in the mid-Miocene and continued in the historical times (Beekman, 1966; Aydar and Gourgaud, 1998; Deniel et al., 1998; Friedrichs et al., 2020a; Kuzucuoğlu et al., 2020). Keçikalesi caldera (13.7 ± 0.3, K-Ar; Besang et al., 1977) has been considered as the oldest stage of Hasandağ stratovolcano (Fig. 1B). The Quaternary products of Hasandağ stratovolcano (including scoria cones, lava domes and two maars) related to Meso-and-Nesovolcano stages (Aydar and Gourgaud, 1998) are mostly located at the summit of the volcano and the NW region known as "Karataş basaltic field" (Ercan et al., 1992; Aydar and Gourgaud, 1998). Most of the basaltic scoria cones are located at the NW and W parts of the volcano, whereas andesitic to dacitic lava domes are formed at the flanks and summit parts (Figs. 1B and 2). The latest activity of Hasandağ stratovolcano around its summit was dated as 8.97 ± 0.64 ka (2σ, U-Th/He on zircons of andesitic pumice; Schmitt et al., 2014). On the other hand, Keçiboyduran volcano is the early Pliocene-Quaternary stratovolcano (e.g. Aydin et al., 2014) located at the eastern part of Hasandağ stratovolcano (Fig. 1B). The basaltic scoria cones and rhyolitic lava domes with related lava flows (224-654 ka, Ar-Ar and U-Pb; Aydin et al., 2014) mostly represent the Quaternary phase of the stratovolcano (Fig. 2).

2.5. Eğrikuyu Monogenetic Field (EMF)

The EMF is an isolated basaltic MVF located at the southern part of Hasandağ stratovolcano and contains numerous scoria cones and a few maars (Notsu et al., 1995; Uslular et al., 2015; Uslular and Gençalioğlu-Kuşcu, 2019b) (Figs. 1B and 2). The clustering of monogenetic vents in the EMF follows two dominant trends, which are generally NE-SW in the west (NE of Karacadağ stratovolcano; 5.98-4.68 Ma; Platzman et al., 1998) and mostly N-S to NW-SE toward the east (between Karacadağ and the south of Hasandağ; Toprak, 1998) (Figs. 1B and 2). Many aligned scoria cones in the region are the possible indication of buried faults (i.e. covered mostly by younger sedimentation and ignimbrite flows) (Toprak, 1998; Uslular et al., 2015). As in the case of other MVFs, there is no clear temporal relationship between the formations of maars and scoria cones based on the available geochronology data (e.g. Kutören maar, 1.31 ± 0.07 Ma, 2σ, Ar-Ar, Reid et al., 2017; scoria cones, 2.60 to 0.30 Ma; Ercan et al., 1992; Notsu et al., 1995; Reid et al., 2017; Doğan-Külahçı et al., 2018).

2.6. Karapınar Monogenetic Field (KMF)

The KMF is another isolated MVF in the southernmost part of the CAVP (Keller, 1974), which was the northeastern margin of the paleolake environment (e.g. Kuzucuoğlu et al., 1999) (Figs. 1B and 2). This region mainly consists of basaltic scoria cones and extensive lava fields (Keller, 1974). However, the presence of dacitic blocky lavas and heterogeneous scoria clasts indicates more complex magmatic processes beneath the region (Keller, 1974). The phreatomagmatic phase in the KMF is represented by a few basaltic maars (i.e. Acıgöl, Mekegölü, Mekeobruğu) and an explosion crater (Yılanobruğu) (Figs. 1B and 2) (Keller, 1974). Maars are probably older than scoria cones (*ca.* 300-390 ka; Reid et al., 2017) as it is revealed by the occurrence of a fresh scoria cone in the middle of Mekegölü maar (Figs. 1B and 2). The general alignment trend in the KMF is NE-SW (Toprak, 1998), which is almost parallel to the Ecemiş fault and elongation of Karacadağ stratovolcano (Figs. 1B and 2). This main trend is also comparable with the general direction of the extension after the late Miocene in the CAVP (Özsayın et al., 2013).

3. Methodology

3.1. Morphological Measurements

The vent database in the CAVP (Toprak, 1998; Arcasoy, 2001; Arcasoy et al., 2004) was firstly revised by selecting the well-preserved monogenetic edifices (i.e. scoria cone, lava dome, and maar), and then filtered based on the types and also relative or absolute ages. Additionally, all the available data in the literature (e.g. geochemistry, geochronology) related to each monogenetic edifice were compiled (Supplementary Material Data-S1). A total of 540 Quaternary monogenetic vents were selected for further analyses performed in this study, but the total number would have exceeded 800 as suggested by Toprak (1998) if non-representative cones/domes (e.g. eroded or too small for morphological studies) and fissures were considered. The morphometric parameters of the most representative scoria cones (174 out of 238) and lava domes (92 out of 195) were measured using the state of the art methodologies suggested in the well-established literature (e.g. Dóniz et al., 2008; Favalli et al., 2009; Karatson et al., 2013; Kereszturi et al., 2013b; Bemis and Ferencz, 2017). We used the Advanced Land Observing Satellite World 3D (AW3D) digital elevation models (DEMs), which are the best freely available ones for the CAVP with a 30 m spatial resolution (5 m height accuracy; Tadono et al., 2015), as a source for morphometric measurements. Most of the monogenetic edifices were omitted either due to their eroded morphology or size below the detection limit (i.e. 30 m resolution AW3D). In addition, 1:25000 scale topographic maps, different satellite and Google Earth images, and fieldwork campaigns further helped us to decipher, when possible, the type of vents within the studied monogenetic volcanoes in the CAVP. Maars are almost 20 in total and their morphological characteristics have been studied in detail using high-resolution drone-based DEMs (Uslular and Gençalioğlu-Kuşcu, 2020). Therefore, we here only focus on the scoria cones and lava domes.

The morphometric measurements of 171 scoria cones and 93 lava domes were performed in the orthogonal directions (i.e. N-S, E-W, NE-SW, and NW-SE) along the monogenetic edifices. The average values are given in Tables 2 and 3. In addition to the basic parameters such as the width of the cone and crater (W_{co} and W_{cr}, respectively), the height of the cone and crater (H_{co} and H_{cr}, respectively), slope and volume, we also classified the types of scoria cones (Dóniz-Páez, 2015; Bemis and Ferencz, 2017) and lava domes (Blake, 1990; Fink and Griffiths, 1998; Aguirre-Díaz et al., 2006; Karatson et al., 2013) (Supplementary Material Data-S1). For the flank cones, we measured the H_{co} values considering the methodology of Favalli et al. (2009). The volumes of both scoria cones and lava domes were calculated by different formulas suggested for the truncated cone shapes (Hasenaka and Carmichael, 1985; Riedel et al., 2003; Kervyn et al., 2012) (Tables 2 and 3). The volumes of ejected materials were also estimated via the empirical relation with the width (d) of the cones and domes ($d_{magmatic} = 0.11\ V_{ejecta}^{0.42}$; Sato and Taniguchi, 1997), and the edifice, ejecta and bulk volumes were corrected by Dense Rock Equivalent (DRE) eruptive volumes (Kereszturi et al., 2013b) (Tables 2 and 3). For the DRE-volume correction of lava domes, the formula suggested for scoria cones (V_{bulk} x 0.4 x 0.5; Kereszturi et al., 2013b) was adopted. The slopes were obtained by both empirical formula (e.g. Bemis and Ferencz, 2017) and DEM-based measurements, and the results of latter method were considered for the further interpretations (Tables 2 and 3). Some additional parameters (i.e. steep-sided-ness, flat-topped-ness, relative crater depth, and crater slope with error estimations) suggested for scoria cones (Bemis and Ferencz, 2017) were also calculated for both scoria cones and lava domes in the CAVP (Tables 2 and 3).

3.2. Fractal Analysis

Many natural phenomena including earthquakes (e.g. Gutenberg and Richter, 1944; Hirabayashi et al., 1992; Legrand, 2002), floods (e.g. Turcotte and Greene, 1993; Malamud and Turcotte, 2006), and volcanoes (e.g. Mazzarini and Armienti, 2001; Ersoy et al., 2007; Pérez-López et al., 2011; Uslular et al., 2015) obey power-law (fractal; Mandelbrot, 1975) frequency-size statistics and hence are considered as fractal (self-similar) features (e.g. Malamud and Turcotte, 1999). The size of volcanic eruptions (i.e. Volcanic Explosivity Index), spatial distribution of volcanic vents (e.g. point-like features), size of scoria cones, and morphology of volcanic ash particles are the common examples of fractal sets in volcanology. Fractal systems (spatial distribution of volcanic vents in our case) are described by non-integer exponent of a power-law function (e.g. Mazzarini and D'Orazio, 2003; and references therein). One of the robust methods to calculate the fractal dimensions is the two-point correlation function method, for the population of N vents, that defines the correlation integral $C_2(l)$ (Grassberger and Procaccia, 1983; Hentschel and Procaccia, 1983; Bonnet et al., 2001) is defined as:

$$C_2(l) = \frac{1}{N^2} N_p(l), \tag{1}$$

where $N_p(l)$ is the number of vent pairs (UTM coordinates) whose separation is less than a given length l. In this cumulative-frequency based definition, $C_2(l)$ is considered as scaled with l in the form of l^{D_2} for the fractal set of vents, where D_2 is the correlation dimension. We hereafter prefer to use the term D_f to be consistent while describing the fractal dimension. If scaling holds in Eq. 1, D is calculated from the slope of a linear regression line in the log $C_2(l)$ vs. log (l) plot (e.g. Bonnet et al., 2001) (Table 4). The fractal dimension D_2 value is calculated in a range of distance on which the function log (C_2) versus log (l) is linear. The lower (L_{co}) and upper (U_{co}) cut-off values (Bonnet et al., 2001), which are the limits between which volcanoes have a fractal distribution, were determined and subsequently used for the interpretation related to crustal mechanism (e.g. Mazzarini, 2004; Mazzarini and Isola, 2010).

3.3. Vent Spacing and Poisson Nearest Neighbor (PNN) Analysis

The coefficient of variation (CV) is mostly used to define homogeneity in the distribution of vents (i.e. CV < 1, regular distribution; CV $= 1$, random or Poisson distribution; CV > 1, clustering of vents; e.g. Mazzarini and Isola, 2010 and references therein). The space (s) between volcanic vents is an important parameter for the understanding of crustal mechanisms (e.g. distribution of fractures) in the adjacent volcanic fields (e.g. Mazzarini, 2007; Mazzarini and Isola, 2010; Mazzarini et al., 2010; 2016) (Table 4). This parameter can be estimated by the Nearest Neighbor (NN) distance method (Clark and Evans, 1954) considering the average minimum distance between vents. The NN method has been commonly used to quantify the spatial distribution of point-like features on Earth and also extraterrestrial settings including volcanic edifices (e.g. scoria and rootless cones; Bruno et al., 2006; Hamilton et al., 2010; Mazzarini et al., 2016; van den Hove et al., 2017). The PNN analysis, as a type of NN method (Baloga et al., 2007), is performed in the MVFs (Connor and Hill, 1995; Le Corvec et al., 2013a) for the understanding of the spatial distribution of vents. Similarly, we applied this method by using the "Geological Image Analysis Software" (GIAS; Beggan and Hamilton, 2010) for the MVFs in the CAVP (Table 5). Details on the methodology for both PNN analysis and GIAS outputs can be found in Le Corvec et al. (2013a; and references therein). The basic parameters (e.g. convex hull, R, c, and skewness) are listed in Table 5. The statistical values R and c, similar to the CV, are the indication of homogeneity in the vent distribution. Ideally, R and c values for a population displaying Poisson distribution are 1 and 0, respectively. However, the more dispersed distributions compared to Poisson display R values > 1, while the more clustered ones have R values < 1 (Beggan and Hamilton, 2010; Le Corvec et al., 2013a). As they are sample-size dependent values, all related diagrams are created within the 2σ uncertainty to overcome this issue (Le Corvec et al., 2013a). The density of vent distribution can also be estimated by considering the ratio between the number of vents (N) and the area of the convex hull (Table 5) (Le Corvec et al., 2013a; Mazzarini et al., 2016).

3.4. Principal Component Analysis (PCA)

The PCA is the most common dimensionality reduction method that has been applied to the spatial data in different aspects of earth sciences (Demšar et al., 2013), including volcanology (Prima and Yoshida, 2010; Mazzarini et al., 2016; Unglert et al., 2016). The original variables are transformed into the new uncorrelated axes that are aligned parallel to the directions of maximum variance in the data (e.g. Demšar et al., 2013) .
In this study, we considered the UTM coordinates of the vents as a pair of variables used in the PCA and followed the steps in Mazzarini et al. (2016) (Table 6). After the dataset is scaled to the barycentre (i.e. the origin of the new dataset is the average values of coordinates), the covariance matrix (Q) of N vents is estimated by:

$$Q = \begin{bmatrix} cov(X,X) & cov(X,Y) \\ cov(X,Y) & cov(Y,Y) \end{bmatrix} \quad , \tag{2}$$

with

$$cov(X,Y) = \sum_{i=1}^{N} \frac{(x_i - \bar{x})(y_i - \bar{y})}{N}, \tag{3}$$

where x_i and y_i are the coordinate values of N vents and their mean values ($\bar{x}$ and $\bar{y}$) are zero as the dataset is translated to barycenter-scaled. The eigenvalues and vectors with the dominant azimuthal direction of the largest eigenvectors are also computed (Mazzarini et al., 2016).

We here aim to provide the shape characteristics of the MVFs in the CAVP using the PCA. The eccentricity (ecc), for instance, relates the lengths of the first and second eigenvectors of the Q (close to 0 and 1, circular or elliptical volcanic fields, respectively) (Table 6). The azimuthal direction of the first eigenvalue of the Q, also considered as a proxy for the field elongation (Table 6), represents the major trend of a long axis for the shape of MVFs (Mazzarini et al., 2016).

3.5. Vent-to-Vent Distance (VVD) Analysis

The preferred azimuthal orientation and/or the anisotropy in vent distribution can be statistically analyzed (e.g. two-point azimuth method, Lutz, 1986; the VVD, Mazzarini et al., 2016) to understand the possible relation between volcano distribution and the tectonic stress fields (e.g. Connor, 1990; Cebriá et al., 2011; Mazzarini et al., 2016; van den Hove et al., 2017). As the vents are considered to be aligned along the same dike or fault (e.g. Takada, 1994), the azimuth values between vents in the MVF are measured. The total number of the segments in the observed set of vent can be expressed as N(N-1)/2, where N is the total number of vents (Wadge and Cross, 1988). The rose diagrams and related histograms of azimuthal distribution in each MVF (Table 6) were used to determine the main peaks (angular error is $\pm$ 3°) and also the angular dispersion ($\Delta\alpha°$; Mazzarini et al., 2016). The unimodal azimuth distribution with a well-defined peak and small $\Delta\alpha(°)$ points to well-aligned vents, while the bimodal distribution with several peaks and large $\Delta\alpha(°)$ refers to the dispersed (or scattered) distribution of vents (Mazzarini et al., 2016).

3.6. Alignment Analysis

In addition to the shape and fractal characteristics of the spatial distribution of monogenetic vents that provide crucial information for the dike networks at the upper crustal level (e.g. Mazzarini, 2004; 2007; Mazzarini and Isola, 2010; Mazzarini et al., 2013), cone elongations and vent alignments are other two important parameters, especially for the understanding of dike orientations (e.g. Tibaldi, 1995; Le Corvec et al., 2013a; Muirhead et al., 2015). In this regard, we here used the morphologies of cones and domes to estimate the possible dike orientations in the upper crust using both observational (Paulsen and Wilson, 2010; Muirhead et al., 2015) and computational (Le Corvec et al., 2013a) methodologies. If the shape reliability of each cone/dome is 1 (probable) or 2 (likely) (Muirhead et al., 2015), and the cone/dome or crater axial ratio (long to short) is above 1.2 (Paulsen and Wilson, 2010), the cone/dome lineaments (i.e. strike of the feeder dyke; Tibaldi, 1995; Muirhead et al., 2015) are recorded. Additionally, the breaching direction of cones is considered as a possible indicator of feeder dyke orientation (Tibaldi, 1995; Muirhead et al., 2015), where the possible reason for breaching is the flow emittance rather than flank collapse or basal inclination (e.g. Németh et al., 2011).

The cone lineament data were further supported by the vent alignment analyses performed by using a MATLAB script of Le Corvec et al. (2013a). Different alignment thicknesses (or width tolerance) were considered (i.e. 11 to 21 with 5 m intervals), which also correspond to the limit of A-grade reliability ($\leq$ 125 m) for the vent alignments suggested by Paulsen and Wilson (2010), and subsequently the best regression lines for each thickness are automatically generated (Le Corvec et al., 2013a). The length tolerance of the alignment, however, is based on the observed cone distribution in each MVF (i.e. the observed mean distances must be less than the estimated ones; Le Corvec et al., 2013a; Muirhead et al., 2015) (Table 5). After all, the alignments are accepted if three vents are aligned within the limits of length tolerance (Fig. 1 of Le Corvec et al., 2013a) and the angular deviation ($\pm$ 15°) of the cone elongation (Paulsen and Wilson, 2010; Muirhead et al., 2015). Additionally, each computed alignments for different thicknesses are displayed on DEMs (AW3D) and different maps of Google Engine using QGIS (Quantum Geographical Information System, version 3.14.15), and those have identical lineament in terms of volcanological evolution are selected. Moreover, the upper limit of the artifact (i.e. ratio of rejected alignments) in each analysis is taken as 10% (Le Corvec et al., 2013a), and hence the maximum distance for the generation of alignment is chosen from those having artifacts $\leq$10% and higher number of alignments. For further details on the methodology of vent alignment analysis briefly mentioned above, Le Corvec et al. (2013a) and Muirhead et al. (2015) can be addressed. In addition, the local and regional fault directions compiled and digitalized from the literature data (Pasquare et al., 1988;

Toprak and Göncüoglu, 1993; Dhont et al., 1998; Froger et al., 1998; Genç and Yürür, 2010) were also displayed on rose diagrams (length weighted) created by using the QGIS plugin "Line Direction Histogram" (Tveite, 2015–2020), and used in comparing the vent and cone/dome alignments with the fault directions and the general extensional trend (N-S to NE-SW; e.g. Özsayın et al., 2013) or regional σ_3 in the CAVP.

4. Results

4.1. Morphological Characteristics

4.1.1. Scoria Cone Morphometry

The morphometric parameters of scoria cones (n = 171) are given in Table 2, and the whole dataset can be found in the Supplementary Material Data-S1. The number of measured scoria cones is the highest in the EMF (Table 2). The NAVC, on the other hand, has the lowest population of scoria cones (Tables 1 and 2). Most of the studied scoria cones (n = 75) are amorphous type (or not bearing crater; Dóniz-Páez, 2015; Bemis and Ferencz, 2017), but the gully and horseshoe-type cones are also abundant (n = 60; Supplementary Material Data-S1). However, ideal-type (Bemis and Ferencz, 2017) or A1-A2 symmetrical ring cones (Dóniz-Páez, 2015) are very rare (n = 13).
The mean absolute errors are included to the results of all morphometric parameters (i.e. mean values), whereas the error limits of ratio-based parameters (i.e. steep-sided-ness, flat-topped-ness) are derived from the empirical formula suggested by Bemis and Ferencz (2017) (Table 2). The width (or basal diameter) of the cones (W_{co}) is the largest in the EVC (696±46 m) and the smallest in the HKVC (583±66 m; Table 2). The height of the cones (H_{co}) changes from 58±10 m in the NAVC to 93±8 m in the EVC (Table 2). However, the largest cone in the CAVP is located within the KMF (Mekedağ; mean H_{co} and W_{co} values are 209 and 1621 m, respectively; Fig. 2 and Supplementary Material Data-S1). Almost half of the measured scoria cones in the CAVP has a crater, and whose width (W_{cr}) is the largest in the KMF (361±45 m) and smallest in the EMF (178±12 m; Table 2). The KMF also has the deepest craters (H_{cr}; 43±5 m), but the lowest values belong to the EMF (14±1 m) and the NAVC (12±4 m; Table 2). Slopes were measured on DEMs, and the mean values (S_{mean}) revealed that the gentle cones (12.3±0.4°) were generally found in the EMF, whereas the steepest ones were located at the EVC (17.4±0.7°) and the KMF (16.9±1.5°; Table 2). For the estimation of cone volume (V_{co})

among the various formulas suggested by different studies (Hasenaka and Carmichael, 1985; Riedel et al., 2003; Kervyn et al., 2012) (Supplementary Material Data-S1), the more commonly used one by Hasenaka and Carmichael (1985) was preferred for further interpretations. The KMF and EVC are the most voluminous fields based on the DRE-corrected (Kereszturi et al., 2013b) V_{co} values (V_{DRE} = 6.9±4.0 x 10^6 m^3 and 6.7±1.4 x 10^6 m^3, respectively), whereas the least voluminous (3.7±1.6 x 10^6 m^3) field is the NAVC as expected due to the sparsity of scoria cones (Table 2). The ejecta volumes of scoria cones were also estimated by using the general formula of Sato and Taniguchi (1997) (W_{cr} = 0.11 $V_{ejecta}^{0.42}$), and the resultant values display comparably more voluminous ejecta deposits in the EVC (5.9±1.5 x 10^8 m^3), but less in the KMF (2.1±0.4 x 10^8 m^3; Table 2). Accordingly, the total volume of scoria cones (V_T) was determined by the summation of cone and ejecta volumes, varying from 2.2±0.4 x 10^8 m^3 in the KMF to 6.0±1.5 x 10^8 m^3 in the EVC (Table 2).

The ratios of morphometric parameters (e.g. H_{co}/W_{co}, W_{cr}/W_{co}; Table 2) and their comparison with the age and volume in conventional binary plots (Fig. 3) were also presented for each MVFs. Fig. 3A displays the relation between H_{co} and W_{co} of the scoria cones, and the slopes (i.e. H_{co}/W_{co}) obtained by the regression lines are all significantly below the so-called ideal ratio (0.18; Wood, 1980), except for a few one that have greater or nearly equal ratios. However, the computed ratios seem to be identical when the recently suggested ratio (H_{mean}/W_{co} = 0.098; Favalli et al., 2009) is considered. This circumstance again highlights the important role of measurement techniques in the morphology studies as previously stated in the literature (e.g. Favalli et al., 2009; Fornaciai et al., 2012). For further interpretations, we preferred to use the shape parameters (i.e. steep-sided-ness and flat-topped-ness; Bemis and Ferencz, 2017) against the traditional ratios, especially due to the fact that steep-sided-ness ($S = 2H_{co}/(W_{co}-W_{cr})$) better represents the flank slopes (Bemis and Ferencz, 2017) . The ideal value of S is 0.6 (31°) that almost corresponds to the traditional ratio of H_{co}/W_{co} (0.18; Wood, 1980). Accordingly, EMF displays the greatest variance in steep-sided-ness (S_{min} = 0.12; S_{max} = 0.64), while the EVC and KMF have generally steep scoria cones (0.31±0.02/0.08 and 0.29±0.03/0.11, respectively; Table 2 and Fig. 3B). Here, x/y type errors correspond to the mean absolute and formula-based (Bemis and Ferencz, 2017) error values, respectively (Table 2). Flat-topped-ness ($F = W_{cr}/W_{co}$) values in the KMF (0.37±0.07) are very close to the ideal ratio of 0.4 (Wood, 1980), whereas those in other clusters vary from 0.23±0.01/0.05 in the EMF to 0.31±0.02/0.05 in the DVC (Table 2). Fig 3B also illustrates that most of the S and F values are moderate, and there are only a few outliers that exceed the ideal ratios. In addition, F values are almost positively correlated with the V_T, whereas the S values have a negative arbitrary trend with the V_T (Figs 3C and D). The compiled age data for the CAVP (Supplementary Material Data-S1) were also compared with the S_{mean} (DEM-based slope) and the S-values (formula-based slope; Bemis and Ferencz, 2017) (Figs. 3E-F). The possible negative trends (i.e. decrease in the slope with the increase in age) could be detected only for the EMF where the number of age data is adequate for comparison (Figs. 3E and F). The DEM-based slopes are comparably better correlated with the age (Fig. 3E). The general output from this correlation is that the flank slopes (especially DEM-based) could be one of the best parameters for the morphometry-based relative dating of scoria cones compared to the common usage of ideal ratios (e.g. H_{co}/W_{co}) that display a rather indistinct correlation (Fig. 3F).

4.1.2. Lava Dome Morphometry

The morphometric parameters of lava domes (n= 91) are summarized in Table 3, and the more comprehensive dataset can be found in the Supplementary Material Data-S1. Lava domes are only found in four MVFs (i.e. EVC, NAVC, DVC, and HKVC), as the KMF and EMF are mainly basaltic MVFs (Fig. 1B). Lava domes are the most abundant in the EVC (n = ∼100), and hence the number of measured domes is highest (n = 56; Table 3). The HKVC has the lowest number of lava domes in the CAVP (n = 11; Table 3). The studied lava domes were also examined in terms of morphological diversity (Blake, 1990; Fink and Griffiths, 1998), and most of them are either platy or spiny (or Pelèan) with many representative examples of lobate and ***coulèe*** types (Fig. 2; Supplementary Material Data-S1). However, some lava domes display complex morphologies, such as Nenezidağ lava dome in the NAVC (92±4 ka; Türkecan et al., 2004 and references therein) with its both spiny and lobate morphology. Dikkartın lava dome in the EVC (10.1±0.8 ka; Sarıkaya et al., 2019) is one of the best examples for coulèe type. Lava domes in the CAVP may also create ridges consisting of aligned spiny domes (e.g. on the flanks of Erciyes stratovolcano in the EVC; Şen et al., 2003; Higgins et al., 2015), or dome complexes (e.g. Korudağ in the NAVC; 24.9±2.1 ka; Schmitt et al., 2011)

(Figs. 1 and 2).

For the morphometric analysis of lava domes, we adopted the common parameters mostly used for scoria cones (Tables 2 and 3). Errors in the morphometric parameters are the mean absolute errors, but the formula-based errors suggested for the shape parameters (i.e. steep-sided-ness, flat-topped-ness; adopted from Bemis and Ferencz, 2017) were also included (Table 3). The height of the domes (H_{do}) varies from 110±21 m in the HKVC to 174±22 m in the DVC (Table 3). Accordingly, the smallest (719±86 m) and largest (1443±176 m) width of the domes (W_{do}) belong to these fields, respectively (Table 3). In Fig. 4A, the H_{do}/W_{do} ratios of each field were compared to those with ideal value of 0.22 (Karatson et al., 2013 and references therein) and different morphologies (i.e. spiny, 0.18; coulèe, 0.17; low, 0.09; Aguirre-Díaz et al., 2006). A considerable number of domes is aligned with the ideal dome ratio, whereas the regression lines of each field are in between low and coulèe type domes (Fig. 4A). Accordingly, the lava domes in the EVC have the highest ratios close to the coulèe and spiny type domes, which is consistent with the observed examples and topography (i.e. flank domes). However, this ratio sharply decreases from the NAVC and DVC (both 0.11) to the HKVC (0.09) (Fig. 4A). Interestingly, the caldera-bearing fields of the NAVC and DVC with numerous resurgent domes have similar ratios, but the HKVC has the lowest, possibly due to a few low-type cones. Similar to the scoria cones, the shape parameters of lava domes from each field were also compared (Fig. 4B). The ideal value of steep-sided-ness (S or flank slope) for scoria cone (0.6; Bemis and Ferencz, 2017) is converted by considering the ideal H_{do}/W_{do} ratio of lava domes (Karatson et al., 2013 and references therein) to estimate an equivalent value (i.e. ~0.7). However, we kept the same ratio of W_{cr}/W_{co} (or flat-topped-ness "F" = 0.4; Wood, 1980) as there is no suggested value for lava domes in the literature. In the measured lava domes, there are only a few domes exceed the ideal ratio of F, but most are located at the mid-range in terms of S-values (Fig. 4B). The EVC and HKVC both including flank domes have the steepest lava domes (0.38±0.01/0.07 and 0.35±0.05/0.08, respectively), whereas the NAVC and DVC have more gently sloping domes (Table 3). In addition, there is relatively positive relation between F and S parameters along with two different trends that might be linked with the age differences. The total volumes of lava domes (V_T) were also compared with these shape parameters (Figs. 4C and D), and the relation is almost positive (especially in S). The most voluminous clusters in terms of lava dome formation are the EVC (8.1±2.0 x 10^7 m^3) and NAVC (8.0±2.4 x 10^7 m^3) compared to other clusters (1.7±0.9 x 10^7 m^3 for the DVC; 2.2±0.7 x 10^7 m^3 for the HKVC; Table 3). As inferred from Fig. 4B, there is a good relation between the slopes of lava domes, especially for those in the NAVC (Figs. 4E and F). Both formula (S) and DEM-based (S_{mean}) flank slopes decrease with the increase of age. However, the same relation for the EVC domes is not valid, and hence there is a need for more age data from the domes in the CAVP to support the possible role of flank slopes in relative dating of domes.

4.2. Self-Similar (Fractal) Clustering

The parameters obtained by the fractal analysis of Quaternary monogenetic vents in the CAVP are listed in Table 4. In addition to the fractal distribution of vents in each MVFs, a total number of scoria cones and lava domes in the CAVP were also analyzed separately in terms of self-similar clustering (Table 4). A plateau in local slope vs. log (l) diagrams could not be well defined for the HKVC and KMF (Fig. 5), either due to the lesser number of vents (e.g. KMF) or spatial distribution of vents or shape characteristics of the volcanic fields. The computed fractal dimensions D_f from the slope of log C_2(l) vs. log(l) plots for other clusters are: 1.16 (NAVC); 1.48 (EMF); 1.55 (EVC); and 1.80 (DVC) (Table 4 and Fig. 5). On the other hand, the scoria cones and lava domes have D_f values of 1.40 and 1.13, respectively (Table 4). The error for the D_f values is almost negligible (i.e. $R^2 = 0.99$). The lower (L_{co}) and upper (U_{co}) cut-off values defined by the size ranges of each vent dataset are also given in Table 4. L_{co} values are very comparable in each MVFs (0.5-0.8 km), while the U_{co} changes from 8.5 km (i.e. shallowest in the DVC) to 16 km (i.e. deepest in the EMF; Table 4 and Fig. 5). The EVC and NAVC have almost similar L_{co} (0.8 km) and U_{co} (10 km and 12 km, respectively) values, indicating a comparable upper crustal mechanism (e.g. depth of brittle-ductile transition) beneath these fields. The values determined for the scoria cones (0.5-15 km) and lava domes (0.7-8 km) are also comparable with the idea of depth difference for the magma source of these edifices (i.e. shallow in lava domes and deeper in scoria cones).

4.3. Vent Spacing and Field Shape Characteristics

The average values of vent spacing/separation (s) in each MVFs are given in Table 4. The maximum average separation (1676 m) was observed in the DVC, while the EVC and NAVC had the minimum values (939 m and 945 m, respectively; Table 4). The mean distances between the vents measured by the PNN analysis (not filtered) also reveal similar results (Table 5). The area of each MVFs defined by a convex hull is also measured, and the EVC and HKVC are the largest volcanic fields in the CAVP (8.68 x 10^8 and 8.55 x 10^8 m^2, respectively; Table 5). These convex hulls were also used for the density calculations (number of vents/m^2), revealing that the density of vent is the highest in the NAVC and EVC (2.39 x 10^{-7} and 2.13 x 10^{-7} m^2) and the lowest in the DVC and HKVC (1.18 x 10^{-7} and 0.91 x 10^{-7} m^2; Table 5). The homogeneity indicators (CV), or the short-range clustering, for the distribution of vents were generally equal or grater than 1 (i.e. clustered distribution; Table 4). However, the results of PNN analysis showed that the NAVC, DVC and KMF have a vent distribution fitting to the Poisson model (Table 5 and Fig. 6). Other clusters display clustered vent distribution (Table 5 and Fig. 6). Although most of the MVFs in the CAVP are nearly circular (≥ 0.70) based on the shape factor (short/long axes of ellipses drawn upon the convex hull), the HKVC and EMF have more elongated shapes (≤ 0.60; Table 5). As the convex hull shape is more sensitive to the outliers, the shape of volcanic fields is then discussed with the results of PCA and VVD analyses.

The field elongations (i.e. eccentricity, *ecc*) and the angular dispersion ($\Delta\alpha°$) obtained by the PCA and VVD analyses do not show a clear relationship, except for the EVC (i.e. vents on the flanks of Erciyes stratovolcano) and the individual MVFs (i.e. EMF and KMF) that display inverse relation (i.e. increase in $\Delta\alpha°$ with the decrease of *ecc*) (Table 6). All the monogenetic clusters have nearly circular elongations (i.e. *ecc* close to 0; Mazzarini et al., 2016; Table 6). In addition, the *ecc* values increase from NE (i.e. 0.03 in the EVC) through the middle part of the CAVP (i.e. 0.28 in the HKVC) towards the SW direction, and then again decrease through the SW-end of the region (i.e. 0.13 in the KMF; Table 6; Fig. 7).

The main azimuthal trends of the vent distribution obtained by both PCA and VVD analyses were compared in each MVFs and also with of the main fault zones in the CAVP (Fig. 7). In addition, we classified these azimuthal vent trends of each MVFs as either normal or parallel/oblique, considering the general extensional direction of the CAVP (N0-90°E; Özsayın et al., 2013). The EVC is the only exceptional case among the other clusters with its almost circular field shape and the radial vent patterns along the flanks of Erciyes stratovolcano (Şen et al., 2003) (Tables 5 and 6 and Fig. 7). The dominant azimuthal trend of vent distribution in the EVC is in the N7°E direction, consistent with the local tectonic stress (e.g. Toprak, 1998; Higgins et al., 2015) and also the genesis of radial dikes (e.g. Nakamura, 1977). On the other hand, the trends in other clusters are generally parallel/oblique to the main extensional direction, except the NAVC that has a trend (N115°) almost parallel/oblique to the TGFZ and perpendicular to the main extension and CAFZ trends (i.e. normal type). In addition, there is a clockwise rotation in the direction of vent alignments from the NAVC to the southern parts (Table 6 and Fig. 7). However, this trend remains mostly constant in the southwestern end of the CAVP (Table 6 and Fig. 7). The PCA and VVD analyses have revealed two important outcomes. The first is the decreasing role of the Tuzgölü fault (NW-SE trend) in the formation of vents that can be spatially followed from the NAVC (normal-type) to the KMF (parallel-type), possibly due to more dominant effect of the regional extensional stress (N-S to NE-SW) with the contribution of CAFZ and/or the role of N-S directed segments in the TGFZ through the southern part (e.g. deformation of Leşkeri scoria cone in the EMF; Toprak and Göncüoglu, 1993; Toprak, 1998) and/or the different behavior of the western and eastern parts of the TGFZ (e.g. Toprak, 1998; Özsayın et al., 2013; Krystopowicz et al., 2020). The second is that the role of the local magmatic stress fields (Muirhead et al., 2015 and references therein) could be a suitable case for the genesis of radial dikes in the EVC considering both tectonic and petrologic characteristics.

4.4. Vent Alignments and Cone/Dome Elongations

The results for the vent alignment analysis in each MVFs are summarized in Table 5. Whole dataset can be found in Supplementary Material Data-S2 and Supplementary Figure SF1. The maximum distance to form the best alignment is determined considering the ratio of rejected alignments (i.e. 10% artifact; Le Corvec et al., 2013a) as illustrated in Supplementary Figure SF1. All detected alignments in the DVC (n=12) and KMF (n=7) are accepted, and therefore there is no artifact in these clusters. However, the number of rejected alignments in other clusters is high, and the accepted lengths of alignments in the EVC, NAVC, HKVC and EMF are 1360, 1552, 2606 and 3738 m, respectively (Table 5 and Supplementary Figure SF1). The number of accepted alignments is highest in the HKVC (n=49) and lowest in the DVC and KMF (Table 5). Most dominant trend in the vent alignments is along the NE-SW direction, which is almost parallel to the main extensional direction (Fig. 7). In the EVC, there is an almost radial pattern of vents that might indicate the effect of the isotropic stress field (e.g. Nakamura, 1977; Nakamura et al., 1977; Paulsen and Wilson, 2009; Marliyani et al., 2020) rather than the regional stress field, or other alternative scenarios (e.g. local magma-induced stress field, volcano overloading; Muirhead et al., 2015 and references therein). However, as also stated in the literature (e.g. Toprak, 1998; Higgins et al., 2015), the dominant trend for the vent alignment in the EVC (n=26; Fig. 7) is N17-38°E, which is almost parallel to the main direction of local faults/lineaments and regional faults and also the extensional direction (Fig. 7). Additionally, there are also vents and faults/lineaments in the EVC with WNW-trend, which are parallel to the NW-directed tensional fractures (Dhont et al., 1998). Vents in the NAVC (n=29; Fig. 7) have NW-SE to N-S trend, almost identical with the main direction of the TGFZ, and perpendicular to the local and regional extension axes. Vents in the DVC (n=12) have almost similar trend (90-130°N) with those in the EVC, which are parallel to the main direction of the local faults and also the northern branch of the CAFZ in the Sultansazlığı pull-apart basin and perpendicular to the local extensional stress field (Fig. 7). In addition, some of the vents, especially those in the eastern part of the DVC, are along with the main trend of Derinkuyu fault (DF; Toprak and Kaymakçı, 1995) (Figs. 1B and 7). The dominant trend for the vent alignments in the HKVC (n=49) is N72-90°E, which is almost parallel to the local extensional stress field (90-95°N; e.g. Genç and Yürür, 2010) and perpendicular to the local and regional faults. The number of detected alignment is higher due to the accumulation of numerous vents (n=25) in the eastern part of the HKVC, which are probably related to the Plio-Quaternary activity of Keçiboyduran stratovolcano (Figs 1B and 2). Contrary to the main trend in the HKVC, the vents in its western part (i.e. Karataş basaltic field; Ercan et al., 1992; Aydar and Gourgaud, 1998) are oriented mostly in the NW-SE direction that reflects the predominant role of the TGFZ in their formation. In the EMF, vents (n=28; Table 5) are mainly aligned with the trend of N45-65°E, which is almost perpendicular to the local extensional stress field (95-100°N; e.g. Genç and Yürür, 2010) and parallel to the main direction of the local faults, the CAFZ (also Ecemiş fault), and the regional extension (Fig. 7). The main trend of aligned vents (n=7) in the KMF is similar with the EMF (N45-65°E), which is almost parallel to the directions of local faults (Fig. 7) and also regional extension but perpendicular to the local extensional stress field (*ca.* 120°N; e.g. Genç and Yürür, 2010).

The elongations of cones and domes are almost identical in all the MVFs in the CAVP, parallel/oblique to the regional extension direction (Fig. 7). The main trend is N70-90°E, except for the KMF where vents are aligned with the direction of N55-75°E (Fig. 7). The role of local and regional faults does not seem to be effective in the formation of cones/domes, but again there is an exception in the KMF where the cone/dome elongation is almost parallel to the main direction of local faults and the CAFZ (also Ecemiş fault) (Fig. 7). The local extensional directions are relatively similar with the cone/dome elongations in the DVC, HKVC and EMF (Fig. 7).

The main results for each MVFs obtained by the analyses mentioned above can be summarized as follows: (i) the vent distribution and alignment in the EVC are mainly controlled by the local and regional extensional stress fields together with the CAFZ; (ii) the NAVC is the only MVF that have a vent distribution/alignment perpendicular to both local and regional extension directions but parallel/oblique to the TGFZ and DF; (iii) the regional extension field and local faults/lineaments seem to be the prevalent mechanisms for the vent distribution/alignments in the DVC; (iv) the local extension field together with the transtensional characteristics of the southern branch of TGFZ mostly shape the vent distribution/alignment in the HKVC; (v) the vent alignments are well observed in the EMF and possibly influenced by various mechanisms (regional extension, local faults/lineaments, and Ecemiş fault); (vi) the number of vents and interrelatedly vent alignments is the least in the KMF, and therefore the interpretations might be misleading. However, the local faults together with the local and regional stress fields seem to be main factors for the vent formation; (vii) the extension parallel/oblique type of direction in the cone/dome elongations (almost E-W) can be explained by both local and regional extensional fields, except the EVC where isotropic stress field is predominant.

5. Discussion

5.1. Morphological Implications

The predominance of dry (i.e. magmatic) eruption style in the monogenetic volcanoes of the CAVP, revealed by the higher number of scoria cones with subordinate lava domes and a few maars (Toprak, 1998), is indirectly supported by our morphological analyses.

In Figs. 3B and 4B, most of the scoria cones and lava domes plot in the lower left panel defined as "arid quadrant" (Fornaciai et al., 2012; Haag et al., 2019) where both S (or traditionally H_{co}/W_{co}) and F (W_{cr}/W_{co}) values are low. The indication of arid regime during the time of monogenetic volcanism in the CAVP is well-correlated with the abundance of scoria cones, but this interpretation may not be valid for the whole CAVP. The reason can be envisioned by two different trends in Fig. 3B in which such relation is better observed due to the higher number of data. For instance, there is a decrease in the S values with the increase of F in the EVC, whereas this relation is almost opposite in the EMF (Fig. 3B). Although these trends are not clear and somewhat scattered, it can refer to the different ratio of phreatomagmatism in the eruption styles (Fornaciai et al., 2012); relatively low in the EVC but high in the EMF, considering the accumulation of eroded deposits at the base of the edifice in dry conditions and the effective erosion or mass wasting in the wet regimes (Fornaciai et al., 2012). This inference is consistent with the paleoenvironmental condition of the southern parts of the CAVP, where the paleolake environments (e.g. Kuzucuoğlu et al., 1999) covered the present boundaries of EMF and KMF. Additionally, this hypothesis is supported by the abundance of maar volcanoes in these MVFs (almost half of the maars in the CAVP; Uslular and Gençalioğlu-Kuşcu, 2020) and also the presence of *Dreissena* sp.-bearing distinct scoria fall deposits in one of the largest scoria cones in the CAVP (Mekedağ scoria cone, KMF; Fig. 2) evident in our field studies. However, as well inferred in the literature (e.g. Kereszturi and Németh, 2012a), such an interpretation does not omit the role of water in the formation of scoria cones, but reveals the predominance of dry-eruption style in their formation with a limited contribution of water as observed in other clusters of the CAVP (e.g. Karnıyarık Hill scoria cone in the DVC; Ersoy et al., 2011).

The morphologies of almost all scoria cones and lava domes are rather different than the ideal edifices (Figs. 3B and 4B). There are only a few possible ideal edifices that have either greater S or F values. This can be explained by several reasons (Fornaciai et al., 2012): (i) the absence of initial ideal cone/dome as in the case of many MVFs (e.g. Kervyn et al., 2012; Bemis and Ferencz, 2017; Haag et al., 2019); (ii) the age discrepancies among the cones/domes and hence different erosional/degradational processes that can also be linked to local climatological conditions. Additionally, the average H_{co}/W_{co} ratio of all measured scoria cones is 0.08, which is within the limit of scoria cones formed in the extensional environments (Fornaciai et al., 2012). This result is in line with the well-known extensional tectonism in the CAVP (e.g. Toprak and Göncüoglu, 1993; Dhont et al., 1998; Genç and Yürür, 2010; Özsayın et al., 2013).

Despite some successful attempts towards the estimation of relative ages based on the cone morphometry (e.g. Inbar et al., 2011; Haag et al., 2019), the use of traditional morphometric ratios (e.g. H_{co}/W_{co}) mostly gives way to misleading interpretations due to the various internal/external effects that control the final morphology (e.g. Kereszturi et al., 2012b; Kereszturi et al., 2013a). Therefore, here we only compared the formula and DEM-based flank slopes of both scoria cones and lava domes with the available radiometric ages to check if there is any meaningful trend or not (Figs. 3E-F and 4E-F). The number of geochronological data for scoria cones is only adequate in the EMF, and thus the possible correlation between ages and flank slopes of scoria cones was tested only for this cluster. Even if the observed relation is not perfect, several negative trends between these variables (i.e. lower slopes in older cones) could be defined. However, additional geochronological data throughout the CAVP, and especially in the EMF, are needed to support this claim.

5.2. Tectonomagmatic Controls on Spatial Vent Distribution

Volcano shape and spatial vent distribution are the best indications for the controlling mechanisms of the tectonic stress fields in the MVFs (e.g. Takada, 1994; Tibaldi, 1995; Brenna et al., 2011; Germa et al., 2013; Le Corvec et al., 2013a; 2015; Muirhead et al., 2015; van den Hove et al., 2017; Haag et al., 2019). Therefore, the spatial distribution analysis of vents certainly provides new insights into the understanding of volcanological evolution and even risk assessments of the MVFs (e.g. Connor et al., 2000; Becerril et al., 2013; Le Corvec et al., 2013a; Mazzarini et al., 2013; 2016; Bertin et al., 2019; Kósik et al., 2020). The shape of volcanic fields (i.e. convex hull; see Table 5), for instance, would be the surface reflection of magma source in the mantle for scoria cones or in the crust for lava domes if the field elongations matched with the vent alignment directions (Le Corvec et al., 2013a). Half of the MVFs (HKVC, EMF, and KMF) within the CAVP have a similar orientation of vent alignments and main field shapes (N88°E, N77°E, and N29°E respectively), and therefore this might indicate that the shallow and deep plumbing systems are mainly controlled by the stress field of crustal scale structures (i.e. fractures). On the other hand, the shape orientations of other clusters (NAVC, N88°E; DVC, N133°) that do not match with the vent alignments are similar to the local extension directions, except for the EVC (N130°) consisting of almost radial patterns of vents (Fig. 7). This might exert that the magma influx in the crust exploits all the possible weaknesses to erupt in the shallow plumbing system, which is probably controlled by the crustal-lithospheric scale structures.

The PNN analysis reveals that half of the MVFs have a clustered distribution (EVC, HKVC, and EMF), while the others display a vent distribution that fits to the Poisson model (non-clustered; Fig. 6). In the clustered vent distribution, the vents are probably formed via a single centralized plumbing system (e.g. Bleacher et al., 2009), which is concordant with the HKVC and EVC (where two stratovolcanoes are exist) and the isolated characteristic of the EMF. For the mechanism of the magma source and its type of activity, it is somehow a challenging task to decide which scenario suggested by Le Corvec et al. (2013a) for the clustered vent distribution can be viable for the MVFs in the CAVP. Although the available age data are rather scarce, the intermittent activity of magma source (low flux and high rejuvenation; Le Corvec et al., 2013a and references therein) seems to be more appropriate especially for the EMF consisting predominantly of scoria cones and a few maars of basaltic composition (Ercan et al., 1992; Notsu et al., 1995; Uslular and Gençalioğlu-Kuşcu, 2019b). However, there are both mafic scoria cones and felsic lava domes within the HKVC and EVC, and thus the hybrid-type activity of magma source (both continuous and discontinuous activity; Le Corvec et al., 2013a and references therein) would be a better mechanism. As for the non-clustered vent distributions, the independent shallow or deep magma reservoirs with low flux and low rejuvenation are the possible sources for the vent formation in these fields (e.g. Bleacher et al., 2009). The bimodal compositions together with various indications for the magma mixing in these MVFs (i.e. NAVC, DVC and KMF) also support this claim. Besides, the presence of both clustered and non-clustered vent distribution within the CAVP is a good indication for the complexity in the geodynamical characteristics of the CAVP.

The main trends of cone elongations (almost E-W) in all MVFs of the CAVP are parallel/oblique to the regional extensional direction (N0-90°E; Fig. 7). However, the vent alignments are distinct and variable in each cluster (Fig. 7). Generally, there are two main preferred or dominant directions of vents defined in almost all the clusters in the CAVP (Fig. 7), that is also suitable with other volcanic regions related to strike-slip (or wrench) tectonism (e.g. Armenia, Pinacate; Le Corvec et al., 2013b and references therein). However, the Kula volcanic field (e.g. Tokçaer et al., 2005; Şen et al., 2014), for instance, located within a pure extensional tectonic regime of the western Anatolia shows clustered vent distribution with more than two main preferred orientations (Le Corvec et al., 2013a). The vents only in the NAVC display almost extension-normal alignment trend, whereas those in other clusters are aligned parallel/oblique to the regional extension axis (Fig. 7). However, when the local extension trends are considered, DVC and EMF have also extension-normal vents (Fig. 7). The extension parallel/oblique lineaments might indicate two main mechanisms for the emplacement of vents (e.g. Le Corvec et al., 2013a; Muirhead et al., 2015), namely the pre-existing structures (e.g. Gudmundsson and Brenner, 2005; Valentine and Krogh, 2006; Le Corvec et al., 2013b) and/or the local rotations of extension direction (or σ_3; e.g. Pollard and Aydin, 1984; Muirhead et al., 2015) throughout the region. As for the CAVP these two mechanisms can be valid, but the latter case seems to be more prevalent as also supported by the structural and paleomagnetism surveys in the region (Dirik and Göncüoglu, 1996; Dhont et al., 1998; Gürsoy et al., 1998; Platzman et al., 1998; Tatar et al., 2000; Piper et al., 2002). However, the role of pre-existing fractures is also obvious in the CAVP, especially revealed by the extension-normal vent alignments in the NAVC where the shortening trend of basement rocks before the late Miocene is NNW-SSE (Göncüoglu et al., 1994). Additionally, the vent and local fault alignments in the DVC and EMF are almost perpendicular to the local extension axes (Fig. 7). The radial vent pattern, on the other hand, was solely observed in the EVC with the main trend of N17-38°E (Fig.7) as also inferred in the literature (Toprak, 1998; Şen et al., 2003; Higgins et al., 2015). The dominant extension-parallel/oblique trend in the EVC can be related to the local rotations of extension direction which is evident by the southward bending of the CAFZ (i.e. lazy S to rhomboidal SSB pull-apart basin, Dirik, 2001; Fig. 8). However, the radial pattern of vents is related to either the effects of the local stress field, probably caused by shallow magma reservoirs in the upper crust and also the mechanical interactions along the fault zones (e.g. Pollard and Aydin, 1984; Gudmundsson, 2006; 2012; Muirhead et al., 2012) and/or major volcano loading (e.g. Van Wyk de Vries and Merle, 1998; Muller et al., 2001; Acocella and Neri, 2009; Le Corvec et al., 2015). Considering the formation of EVC along the CAFZ border fault and also the existence of many indications for the shallow magma reservoirs beneath the region (Fig. 8), both mechanisms can be valid for the radial emplacement of vents in the EVC. On the other hand, the MVFs close to the TGFZ border fault has been under the effect of this fault zone whose role possibly decreases through the southern parts of the CAVP (or the normal fault kinematic of the TGFZ increases).

5.3. Geodynamical Perspectives: Special Reference to Crustal Structures

Central Anatolia is an important part of the escape tectonism in the Anatolia (possibly commenced at early Pliocene; e.g. Faccenna et al., 2006) when there is a westward movement by lateral extrusion after the collision between Arabian and Eurasian plates along the Bitlis Suture Zone during the middle Miocene (e.g. Şengör et al., 1985; Okay et al., 2010; Philippon et al., 2014; Cavazza et al., 2018). The initiation of widespread volcanism in the CAVP slightly postdates this collision based on the available geochronology data (i.e. Keçikalesi caldera, 13.7 ± 0.3 Ma; Besang et al., 1977), and has been directly influenced by the tectonic changes during its evolution (e.g. Toprak and Göncüoglu, 1993; Dirik and Göncüoglu, 1996; Dhont et al., 1998; Froger et al., 1998; Toprak, 1998). Two border fault zones, the TGFZ (e.g. Çemen et al., 1999) and CAFZ (e.g. Koçyiğit and Beyhan, 1998) (Fig. 8), exert the main control especially for the widespread Plio-Quaternary volcanism in the CAVP, either by triggering the volcanism (e.g. Gençalioğlu-Kuşcu and Geneli, 2010) or just being used as a pathway for the magma enroute to the surface (e.g. Toprak, 1998; Abgarmi et al., 2017). This might be tested, for instance, by the chondrite normalized values of CAVP basalts (Uslular and Gençalioğlu-Kuşcu, 2019a) on the Sm vs. La/Sm diagram (Supplementary Figure SF2). The main tendency of the CAVP basalts is along the source variation pattern, which also favours the idea of mantle heterogeneity (Reid et al., 2017; Uslular and Gençalioğlu-Kuşcu, 2019b). Intra-continental faults that might project to the base of the lithosphere result in the decompression melting with batch modelling processes (e.g. Cas et al., 2017). Therefore, considering the evidence of decompression melting (Gençalioğlu-Kuşcu and Geneli, 2010) and the conflicts in the possible mechanisms of asthenospheric upwelling in the CAVP (e.g. Delph et al., 2017; Rabayrol et al., 2019), the mechanism controlled by the lithospheric-scale CAFZ (Fig. 8) can be a viable scenario for the evolution of CAVP volcanism. Alternatively, the CAFZ together with the crustal-depth TGFZ displaying various strike-slip structures (e.g. en-echelon structures, releasing bends; e.g. Dirik and Göncüoglu, 1996, Koçyiğit and Beyhan, 1998; Dirik, 2001) have certainly given a way to the propagation of magma during the evolution of the CAVP (especially after late Pliocene).

Together with the anticlockwise rotation occurred in two successive temporal stages after the collision (i.e. crustal thickening up to the late Pliocene and subsequently the acceleration of rotation due to escape tectonics; e.g. Gürsoy et al., 1998; Tatar et al., 2000; Piper et al., 2002; Gürsoy et al., 2003), the strike-slip fault (or wrench) tectonism appears to be one the most suitable geodynamic models for the recent landscape of the CAVP (e.g. Aydemir, 2009). Unlike the trend of regional crustal rotation, the vent alignments display spatial variations throughout the CAVP (Fig. 7). When the TGFZ is considered as a boundary, the MVFs in its northern parts (i.e. the NAVC and DVC) display clockwise rotation in the vent alignments through the HKVC that juxtaposes the TGFZ (Fig. 7). However, this trend turns slightly anticlockwise in the southern part of the TGFZ for the vent alignments of the EMF and KMF (Fig. 7). In addition to the possible role of the CAFZ and local faults, the southerly change in the direction of vent alignment may reflect the spatial variations in the characteristics of the TGFZ that are also linked to the various crustal- and lithospheric-scale processes (e.g. crustal rotation and heating, tectonic escape, uplifting; Krystopowicz et al., 2020 and references therein). As for the EVC, both extension-parallel/oblique main trend and the general radial pattern of the vents proclaim that this part of the CAVP behaves like an immature rift zone (e.g. Acocella, 2014; Muirhead et al., 2015) where EVC can be the magmatic transfer zone. This claim is also supported by the vent alignments of NAVC and DVC (i.e. almost extension-normal) that can be considered as the boundary between the so-called transfer zone (i.e. CAFZ) and the distal end of the so-called rift basin (i.e. TGFZ). The vent alignments in these regions are mainly controlled by the regional extensional stress fields (Muirhead et al., 2015). Similar to the vent alignments (Fig. 7), the spatial variation in the *ecc*-values (i.e. field elongations; Table 6) also corroborates the above claim, and there is a significant increase in the *ecc*-values from EVC through the NAVC and DVC up to the HKVC, followed by the decrease throughout the southern ends of the CAVP.

Such variation is well-documented in the main Ethiopian rift, for example, where the *ecc*-values increase from the rift border to the main axis (Mazzarini et al., 2016).

Fig. 8 illustrates the probable crustal- and mantle dynamics beneath the CAVP. The type of interaction between lithospheric and asthenospheric mantle, i.e. either melt percolation (Rabayrol et al., 2019) or dripping (e.g. Göğüş et al., 2017; Reid et al., 2017) lies beyond the scope of this manuscript. However, the westward propagation of slab break-off in the sinking Arabian segment of the southern Neotethyan slab (e.g. Biryol et al., 2011; Cosentino et al., 2012; Schildgen et al., 2014; Rabayrol et al., 2019) has mostly controlled the mid-Miocene to recent volcanism in the CAVP. This migration also resulted in the uplifting of southern central Anatolia and also significant changes in the retreat rates of the Cyprus (i.e. slowing) and Hellenic (i.e. speeding) trenches (e.g. Schildgen et al., 2014) (Fig. 1A). Interrelatedly, the dominant N-S convergence in the central Anatolia gave way to the NE-SW extension in the late Miocene (e.g. Özsayın et al., 2013; Schildgen et al., 2014), and its consequences together with the triggering of border fault zones (i.e. TGFZ and CAFZ) via tectonic escape in the late Pliocene (e.g. Faccenna et al., 2006) directly controlled the widespread volcanism in the CAVP (e.g. Toprak and Göncüoglu, 1993; Dhont et al., 1998; Toprak, 1998; and this study). Within this scenario, the CAFZ, which is situated at the near eastern boundary of the Inner Tauride suture zone (Fig. 1A), has a distinct role in the propagation of mantle-derived melts enroute to the surface and behaves like an immature rift zone together with the EVC (i.e. magmatic transfer zone). This interpretation is well-documented in our multivariate statistical and alignment analysis of vents in the CAVP. On the other hand, the TGFZ as a western border fault zone in the region has mostly played a role in the crustal propagation of the magma to the surface (e.g. Toprak and Göncüoglu, 1993; Dirik and Göncüoglu, 1996; and this study). Additionally, the spatial changes in the kinematic of the TGFZ (i.e. changes from almost pure strike-slip in the NW to a transtensional in the SE; e.g. Krystopowicz et al., 2020) mostly shaped the vent alignments in the central (NAVC, DVC) and southwestern parts (EMF, KMF) of the CAVP (Fig. 7).

The hot upper mantle with the very slow shear velocities ($\leq$4.2 km/s; Delph et al., 2017) beneath the CAVP has been well-documented (e.g. Biryol et al., 2011; Abgarmi et al., 2017; Reid et al., 2017; Artemieva and Shulgin, 2019). The low-velocity anomalies tentatively illustrated in Fig. 8 around 20 km (e.g. Abgarmi et al., 2017) display a good correlation with the widespread volcanism in the CAVP. The compiled earthquake data from the central Anatolia (Supplementary Figure SF3) also indicate the possible depth of brittle-ductile transition as around 16-20 km (with the maximum events in 8-10 km) beneath the CAVP (Fig. 8). Additionally, we interpreted this transition and also the depth of dike intrusions with the results of our fractal analysis, considering the U_{co} values (Table 4; Fig. 5). Accordingly, these interpretations are interestingly well correlated with the available geophysical studies. For instance, the Curie depths are lower beneath the NAVC and DVC ($\leq$10 km; Ateş et al., 2005) where U_{co} values are 12 and 8.5 km, respectively (Fig. 8). Also, the deepest U_{co} value of the EMF (16 km) conforms with the Curie depths in this region ($\geq$15 km; Ateş et al., 2005). A similar interpretation was not possible for the HKVC and KMF due to the lack of acceptable local slopes in their fractal analysis (Fig. 5). Therefore, the depth of possible dike intrusions beneath the HKVC could only be adopted from a recent magnetotelluric study of Tank and Karaş (2020). On the other hand, there is no data for the KMF, and hence the possible depth could not be directly estimated. As an alternative to all mentioned above related to the fractal outputs, the variation of U_{co} values throughout the CAVP can only be the indication of slight spatial differences in the crustal thickness and/or the depth of brittle-ductile transition. However, in both scenarios, there is a significant role of crustal lithology (e.g. van den Hove et al., 2017) that shows a spatial difference in the CAVP (i.e. soft-substrata sedimentary basins in the south of TGFZ, Ereğli plain and Ulukışla basin, e.g. Clark and Robertson, 2005; Gürbüz et al., 2020; hard-substrata crystalline basement rocks in the north, namely Kırşehir block; Okay and Tüysüz, 1999).

6. Concluding Remarks

Our detailed analyses for the morphology and spatial distribution of monogenetic volcanoes in the CAVP using multivariate statistical methods lead us to conclude that:

- The six MVFs defined in the CAVP display almost all types of scoria cones (e.g. gully, horseshoe, tilted, crater row), lava domes (e.g. spiny, lobate, and coulèe), and maars. In terms of both scoria cones and lava domes, the Erciyes Volcanic Complex is the most voluminous MVFs (V_T=6.0±1.5E+08 m^3) in the CAVP. The lower morphological ratios such as steep-sided-ness and flat-topped-ness indicate that the magmatic eruptions are predominate compared to phreatomagmatic ones. The defined types of monogenetic volcanoes in the CAVP also support this claim (i.e. mostly scoria cones with subordinate lava domes, and a few maars and tuff rings). Among the various morphometric parameters, the flank slopes either calculated by formulas or DEMs are the best that show well correlation with the limited geochronological data, and therefore they might be promoted to be used in further relative dating studies. However, there is still a need for more absolute age data to support this claim. The crustal lithology (e.g. soft vs. hard substrata) and fracture network mostly control the morphological variations together with the generally known internal and external factors (e.g. vesicularity, composition, climate, and erosion).

- Most of the MVFs in the CAVP except the Hasandağ-Keçikalesi Volcanic Complex and Karapınar Monogenetic Field have a fractal distribution in space. The fractal dimensions (D_f) are different for each MVF, probably because of the discrepancies in the crustal thickness and the fracture network. The U_{co} values here are considered as an initial depth of dike intrusions, and display spatial variations; the highest (16 km) corresponds to the Eğrikuyu Monogenetic Field situated in the south of the Tuz Gölü Fault Zone, whereas the lowest corresponds to the northern parts (8.5 to 12 km). These values are well-correlated with the available geophysical anomalies (e.g. low-velocity, Curie depth) and the depth of brittle-ductile transition in the crust (16- 20 km) confirmed by the earthquake catalogue of the region.

- The PNN analysis showed that both clustered and non-clustered vent distributions (centralized and single plumbing systems, respectively) are observed in the CAVP. The isolated basaltic Eğrikuyu Monogenetic Field and the bimodal Hasandağ-Keçikalesi and Erciyes Volcanic Complexes consisting of two major stratovolcanoes display a clustered vent distribution, while the bimodal Nevşehir-Acıgöl and Derinkuyu Volcanic Complexes together with the Karapınar Monogenetic Field bearing the trace of mingling/mixing in lava flows have a non-clustered vent distribution. In accordance with the crustal lithology and fracture network, the propagation of mantle-derived magma sources is probably intermittent (low flux high rejuvenation) in the Eğrikuyu Monogenetic Field where the basaltic volcanism predominates. However, both continuous and intermittent (hybrid-type) activities can be valid for the Hasandağ-Keçikalesi and Erciyes Volcanic Complexes considering the presence of mafic scoria cones and felsic lava domes together. On the other hand, the MVFs displaying non-clustered vent distribution have single magma reservoirs with low flux and low rejuvenation.

- The vent alignment and cone/dome elongation analyses provide three different patterns, two single orientations (extension-normal and extension-oblique/parallel) and a radial pattern. The first orientation is in the continuation of the regional extensional axis near the Tuz Gölü Fault Zone. Located at the central part of the CAVP, the second orientation is nearly normal to the regional extension axis, possibly indicating the increasing role of pre-existing fractures in the vent formation. The third pattern, located at the Erciyes Volcanic Complex, is radial with a main trend of N17-38°E. We also observe that the *ecc*-values increase from the Erciyes Volcanic Complex to the Hasandağ-Keçikalesi Volcanic Complex, and decrease in the south part of the Tuz Gölü Fault Zone. Hence demonstrating that the spatial distribution of the CAVP vents is controlled by the pre-existing fractures, the extensional axis of the regional stress tensor, and the local stress field variations.

- As inferred in the recent literature, we also agree that the asthenospheric source presents beneath the CAVP is probably related to the slab-tearing processes that occurred in the Anatolian segment of the Neo-Tethyan slab, rather than the Cyprus segment, around the mid-Miocene and subsequently propagated westward in the late Pliocene. Accordingly, the processes during and after the collision along the Bitlis Suture Zone have mostly controlled the whole volcanic evolutionary history of the CAVP; i.e. mid-to-late Miocene volcanism mostly controlled by the N-S convergence with a significant crustal thickening, and the later extension-related Plio-Quaternary volcanism mostly governed by the reactivated border fault zones due to the westward tectonic escape. In each stage, the Central Anatolian Fault Zone involving some typical strike-slip components (e.g. en-echelon structures and a releasing bend) and juxtaposing with the Inner Tauride Suture Zone that either triggers the melting and asthenospheric upwelling or not is the region where the mantle-derived magmas are transported to the surface. Therefore, the Erciyes Volcanic Complex occurred along the Central Anatolian Fault Zone is also considered as a magmatic transfer zone in the Plio-Quaternary period of CAVP volcanism, and mostly controls the spatial distribution of the vents with the significant help of crustal-level Tuz Gölü Fault Zone and other tectonic features.

- Our recent findings related to the interaction between tectonism and volcanism revealed by the detailed multivariate statistical and alignment analyses will certainly provide new insights into the understanding of the Plio-Quaternary volcanism in the CAVP. Additionally, these more quantitative outputs will surely be evaluated in the volcanic risk assessment studies recently intended for the CAVP. Possible applications of similar approaches to the other Quaternary volcanic regions within the Anatolia would also be remarkable to create a better constraint for the evolution of the Quaternary volcanism throughout the region.

Acknowledgements

All graphs except for PNN and PCA analyses were prepared by using Veusz (python-based scientific plotting program; Sanders, 2008). We also acknowledge the freely available QGIS software that enabled us to create maps and perform some analysis (e.g. calculation of azimuth, drawing rose diagrams) using its comprehensive toolbox and various add-ins.

Supplementary Material

Supplementary Data-S1. Morphological dataset of Quaternary scoria cones and lava domes in the CAVP

Supplementary Data-S2. Alignment analysis results for each MVFs in the CAVP

Supplementary Figure SF1

Supplementary Figure SF2

Supplementary Figure SF3

References

Abgarmi, B., Delph, J.R., Ozacar, A.A., Beck, S.L., Zandt, G., Sandvol, E., Turkelli, N., Biryol, C.B., 2017. Structure of the crust and African slab beneath the central Anatolian plateau from receiver functions: New insights on isostatic compensation and slab dynamics. Geosphere 13, 1774–1787.

Acocella, V., 2014. Structural control on magmatism along divergent and convergent plate boundaries: Overview, model, problems. Earth-Sci. Rev. 136, 226–288.

Acocella, V., Neri, M., 2009. Dike propagation in volcanic edifices: overview and possible developments. Tectonophysics 471, 67–77.

Aguirre-Díaz, G.J., del Carmen Jaimes-Viera, M., Nieto-Obregón, J., 2006. The Valle de Bravo Volcanic Field: Geology and geomorphometric parameters of a Quaternary monogenetic field at the front of the Mexican Volcanic Belt. In: Siebe, C., Macías, J.L., Aguirre-Díaz, G.J., (Eds.), Neogene-Quaternary continental margin volcanism: A perspective from México. Geol. Soc. Am., 402, 139–154.

Arcasoy, A., 2001. A new method for detecting the alignments from point-like features: an application to the volcanic cones of Cappadocian Volcanic Province, Turkey. Ph.D. thesis. Middle East Technical University, Ankara, 157p.

Arcasoy, A., Toprak, V., Kaymakçı, N., 2004. Comprehensive Strip Based Lineament Detection Method (COSBALID) from point-like features: a GIS approach. Comput. and Geosci. 30, 45–57.

Artemieva, I.M., Shulgin, A., 2019. Geodynamics of Anatolia: Lithosphere thermal structure and thickness. Tectonics 38, 4465–4487.

Asan, K., Kurt, H., 2011. Petrology and Geochemistry of Post-Collisional Early Miocene Volcanism in the Karacadağ Area (Central Anatolia, Turkey). Acta Geol. Sin. 85, 1100–1117.

Atıcı, G., Schmitt, A.K., Friedrichs, B., Sparks, S., Danišík, M., Yurteri, E., Gündoğdu, E.A., Schindlbeck-Belo, J., Çobankaya, M., Wang, K.L., et al., 2019. Ages and glass compositions for paired large-volume eruptions from the Acigöl volcanic complex, Cappadocia (Turkey). Med. Geo. Rev. 1, 167–178.

Ateş, A., Bilim, F., Buyuksarac, A., 2005. Curie point depth investigation of Central Anatolia, Turkey. Pure. Appl. Geophys. 162, 357–371.

Aydar, E., Gourgaud, A., 1998. The geology of Mount Hasan stratovolcano, central Anatolia, Turkey. J. Volcanol. Geoth. Res. 85, 129–152.

Aydar, E., Schmitt, A.K., Çubukçu, H.E., Akin, L., Ersoy, O., Sen, E., Duncan, R.A., Atici, G., 2012. Correlation of ignimbrites in the central Anatolian volcanic province using zircon and plagioclase ages and zircon compositions. J. Volcanol. Geoth. Res. 213, 83–97.

Aydar, E., Şen, E., Sarıkaya, M.A., Kuzucuoğlu, C., 2019. In the Footsteps of Strabon: Mount Erciyes Volcano—The Roof of Central Anatolia and Sultansazliği Basin, in: Landscapes and Landforms of Turkey. Springer, pp. 565–576.

Aydar, E., Çubukçu, E., Ulusoy, I., Ersoy, O., Sen, E., Yürür, M., Ekmekçi, M., Atıcı, G., Atak, O., Kabadayı, E., Akın, L., 2011. Nevşehir Kalderası'nın Volkanolojik-Petrolojik Evriminin ve Tektonizma-Volkanizma İlişkisinin Zaman ve Mekan İçinde İncelenmesi. Technical Report. TÜBİTAK Project No. 108Y063 (Turkish with English Abstact).

Aydemir, A., 2009. Tectonic investigation of Central Anatolia, Turkey, using geophysical data. J. Appl. Geophys. 68, 321–334.

Aydin, F., Schmitt, A.K., Siebel, W., Sönmez, M., Ersoy, Y., Lermi, A., Dirik, K., Duncan, R., 2014. Quaternary bimodal volcanism in the Niğde Volcanic Complex (Cappadocia, central Anatolia, Turkey): age, petrogenesis and geodynamic implications. Contrib. Mineral. Petrol. 168, 1078.

Baloga, S., Glaze, L., Bruno, B., 2007. Nearest-neighbor analysis of small features on Mars: Applications to tumuli and rootless cones. J. Geophys. Res. Planets 112.

Bartol, J., Govers, R., 2014. A single cause for uplift of the Central and Eastern Anatolian plateau? Tectonophysics 637, 116–136.

Becerril, L., Cappello, A., Galindo, I., Neri, M., Del Negro, C., 2013. Spatial probability distribution of future volcanic eruptions at El Hierro Island (Canary Islands, Spain). J. Volcanol. Geoth. Res. 257, 21–30.

Beekman, P.H., 1966. The Pliocene and quaternary volcanism in the Hasan Dağ-Melendiz Dağ region. Maden Tetkik ve Arama Dergisi 66.

Beggan, C., Hamilton, C.W., 2010. New image processing software for analyzing object size-frequency distributions, geometry, orientation, and spatial distribution. Comput. and Geosci. 36, 539–549.

Bemis, K.G., Ferencz, M., 2017. Morphometric analysis of scoria cones: the potential for inferring process from shape. Geol. Soc. Spec. Publ. 446, 61–100.

Bertin, D., Lindsay, J.M., Becerril, L., Cronin, S.J., Bertin, L.J., 2019. MatHaz: a Matlab code to assist with probabilistic spatio-temporal volcanic hazard assessment in distributed volcanic fields. J. Appl. Volcanol. 8, 4.

Besang, C., Eckhardt, F., Harre, W., Kreuzer, H., Müller, P., 1977. Radiometrische altersbestimmungen an Neogenen eruptivgesteinen der Türkei. Geol. Jahr. 25, 3–36.

Biryol, C., Beck, S.L., Zandt, G., Özacar, A.A., 2011. Segmented African lithosphere beneath the Anatolian region inferred from teleseismic P-wave tomography. Geophys. J. Int. 184, 1037–1057.

Blake, S., 1990. Viscoplastic models of lava domes, in: Lava flows and domes. Springer, pp. 88–126.

Bleacher, J.E., Glaze, L.S., Greeley, R., Hauber, E., Baloga, S.M., Sakimoto, S.E., Williams, D.A., Glotch, T.D., 2009. Spatial and alignment analyses for a field of small volcanic vents south of Pavonis Mons and implications for the Tharsis province, Mars. J. Volcanol. Geoth. Res. 185, 96–102.

Bonnet, E., Bour, O., Odling, N.E., Davy, P., Main, I., Cowie, P., Berkowitz, B., 2001. Scaling of fracture systems in geological media. Rev. Geophys. 39, 347–383.

Brenna, M., Cronin, S.J., Nemeth, K., Smith, I.E., Sohn, Y.K., 2011. The influence of magma plumbing complexity on monogenetic eruptions, Jeju Island, Korea. Terra Nova 23, 70–75.

Bruno, B.C., Fagents, S., Hamilton, C.W., Burr, D., Baloga, S., 2006. Identification of volcanic rootless cones, ice mounds, and impact craters on Earth and Mars: Using spatial distribution as a remote sensing tool. J. Geophys. Res. Planets 111.

Cañón-Tapia, E., 2020. Influence of method selection on clustering analyses of point-like features: Examples from three zones of distributed volcanism. Geomorphology 354, 107063.

Cas, R., Van Otterloo, J., Blaikie, T., Van Den Hove, J., 2017. The dynamics of a very large intra-plate continental basaltic volcanic province, the Newer Volcanics Province, SE Australia, and implications for other provinces. Geol. Soc. Spec. Publ. 446, 123–172.

Cavazza, W., Cattò, S., Zattin, M., Okay, A.I., Reiners, P., 2018. Thermochronology of the Miocene Arabia-Eurasia collision zone of southeastern Turkey. Geosphere 14, 2277–2293.

Cebriá, J., Martín-Escorza, C., López-Ruiz, J., Morán-Zenteno, D., Martiny, B., 2011. Numerical recognition of alignments in monogenetic volcanic areas: Examples from the Michoacán-Guanajuato Volcanic Field in Mexico and Calatrava in Spain. J. Volcanol. Geoth. Res. 201, 73–82.

Clark, M., Robertson, A., 2005. Uppermost Cretaceous–Lower Tertiary Ulukışla Basin, south-central Turkey: sedimentary evolution of part of a unified basin complex within an evolving Neotethyan suture zone. Sediment. Geol. 173, 15–51.

Clark, P.J., Evans, F.C., 1954. Distance to nearest neighbor as a measure of spatial relationships in populations. Ecology 35, 445–453.

Connor, C.B., 1987. Structure of the Michoacán-Guanajuato volcanic field, Mexico. J. Volcanol. Geoth. Res. 33, 191–200.

Connor, C.B., 1990. Cinder cone clustering in the TransMexican Volcanic Belt: implications for structural and petrologic models. J. Geophys. Res-Sol. Ea. 95, 19395–19405.

Connor, C.B., Hill, B.E., 1995. Three nonhomogeneous Poisson models for the probability of basaltic volcanism: application to the Yucca Mountain region, Nevada. J. Geophys. Res-Sol. Ea. 100, 10107–10125.

Connor, C.B., Stamatakos, J.A., Ferrill, D.A., Hill, B.E., Ofoegbu, G.I., Conway, F.M., Sagar, B., Trapp, J., 2000. Geologic factors controlling patterns of small-volume basaltic volcanism: Application to a volcanic hazards assessment at Yucca Mountain, Nevada. J. Geophys Res-Sol. Ea. 105, 417–432.

Cosentino, D., Schildgen, T.F., Cipollari, P., Faranda, C., Gliozzi, E., Hudáčková, N., Lucifora, S., Strecker, M.R., 2012. Late Miocene surface uplift of the southern margin of the Central Anatolian Plateau, Central Taurides, Turkey. Bulletin 124, 133–145.

Çemen, I., Göncüoglu, M.C., Dirik, K., 1999. Structural evolution of the Tuzgölü basin in Central Anatolia, Turkey. J. Geol. 107, 693–706.

Çiner, A., Aydar, E., 2019. A fascinating gift from volcanoes: the fairy chimneys and underground cities of Cappadocia, in: Landscapes and Landforms of Turkey. Springer, pp. 535–549.

Çiner, A., Doğan, U., Yıldırım, C., Akçar, N., Ivy-Ochs, S., Alfimov, V., Kubik, P.W., Schlüchter, C., 2015. Quaternary uplift rates of the Central Anatolian Plateau, Turkey: insights from cosmogenic isochron-burial nuclide dating of the Kızılırmak River terraces. Quat. Sci. Rev. 107, 81–97.

Delph, J.R., Abgarmi, B., Ward, K.M., Beck, S.L., Özacar, A.A., Zandt, G., Sandvol, E., Türkelli, N., Kalafat, D., 2017. The effects of subduction termination on the continental lithosphere: Linking volcanism, deformation, surface uplift, and slab tearing in central Anatolia. Geosphere 13, 1788–1805.

Demšar, U., Harris, P., Brunsdon, C., Fotheringham, A.S., McLoone, S., 2013. Principal component analysis on spatial data: an overview. Ann. Am. Assoc. Geogr. 103, 106–128.

Deniel, C., Aydar, E., Gourgaud, A., 1998. The Hasan Dagi stratovolcano (Central Anatolia, Turkey): evolution from calc-alkaline to alkaline magmatism in a collision zone. J. Volcanol. Geoth. Res. 87, 275–302.

Dhont, D., Chorowicz, J., Yürür, T., Froger, J.L., Köse, O., Gündogdu, N., 1998. Emplacement of volcanic vents and geodynamics of Central Anatolia, Turkey. J. Volcanol. Geoth. Res. 85, 33–54.

Di Giuseppe, P., Agostini, S., Manetti, P., Savaşçın, M.Y., Conticelli, S., 2018. Sub-lithospheric origin of Na-alkaline and calc-alkaline magmas in a post-collisional tectonic regime: Sr-Nd-Pb isotopes in recent monogenetic volcanism of Cappadocia, Central Turkey. Lithos 316, 304–322.

Dirik, K., 2001. Neotectonic evolution of the northwestward arched segment of the Central Anatolian Fault Zone, Central Anatolia, Turkey. Geol. Acta 14, 147–158.

Dirik, K., Göncüoglu, M.C., 1996. Neotectonic characteristics of central Anatolia. Int. Geol. Rev. 38, 807–817.

Doğan-Külahçı, G.D., Temel, A., Gourgaud, A., Varol, E., Guillou, H., Deniel, C., 2018. Contemporaneous alkaline and calc-alkaline series in Central Anatolia (Turkey): Spatio-temporal evolution of a post-collisional Quaternary basaltic volcanism. J. Volcanol. Geoth. Res. 356, 56–74.

Dóniz, J., Romero, C., Coello, E., Guillén, C., Sánchez, N., García-Cacho, L., García, A., 2008. Morphological and statistical characterisation of recent mafic volcanism on Tenerife (Canary Islands, Spain). J. Volcanol. Geoth. Res. 173, 185–195.

Dóniz-Páez, J., 2015. Volcanic geomorphological classification of the cinder cones of Tenerife (Canary Islands, Spain). Geomorphology 228, 432–447.

Druitt, T., Brenchley, P., Gökten, Y., Francaviglia, V., 1995. Late Quaternary rhyolitic eruptions from the Acigöl Complex, central Turkey. J. Geol. Soc. 152, 655–667.

Ercan, T., Tokel, S., Matsuda, J.I., Ui, T., Notsu, K., Fujitani, T., 1992. Hasandağı-Karacadağ (Orta Anadolu) Kuvaterner Volkanizmasına İlişkin Yeni Jeokimyasal, İzotopik ve Radyometrik Veriler. Türkiye Jeoloji Kurultayı Bülteni 7, 8–21.

Ersoy, O., Aydar, E., Gourgaud, A., Artuner, H., Bayhan, H., 2007. Clustering of volcanic ash arising from different fragmentation mechanisms using Kohonen self-organizing maps. Comput. and Geosci. 33, 821–828.

Ersoy, O., Aydar, E., Şen, E., Gourgaud, A., 2019. Contrasting fragmentation and transportation dynamics during the emplacement of Dikkartın rhyodacitic dome; Erciyes stratovolcano, central Turkey. Med. Geo. Rev. 1, 223–242.

Ersoy, O., Aydar, E., Sen, E., Ulusoy, I., Cubukcu, E., 2011. Göllüdağ-Acıgöl (Kapadokya Volkanik Provensi) Bölgesinde Yer Alan Bir Cüruf Konisinin Patlama ve Yerleşme Dinamiklerinin Saptanması. Technical Report. TÜBİTAK Project No. 109Y169 (Turkish with English Abstact).

Faccenna, C., Bellier, O., Martinod, J., Piromallo, C., Regard, V., 2006. Slab detachment beneath eastern Anatolia: A possible cause for the formation of the North Anatolian fault. Earth. Planet. Sc. Lett. 242, 85–97.

Favalli, M., Karátson, D., Mazzarini, F., Pareschi, M.T., Boschi, E., 2009. Morphometry of scoria cones located on a volcano flank: a case study from Mt. Etna (Italy), based on high-resolution LiDAR data. J. Volcanol. Geoth. Res. 186, 320–330.

Fink, J.H., Griffiths, R.W., 1998. Morphology, eruption rates, and rheology of lava domes: Insights from laboratory models. J. Geophys. Res-Sol. Ea. 103, 527–545.

Fornaciai, A., Favalli, M., Karátson, D., Tarquini, S., Boschi, E., 2012. Morphometry of scoria cones, and their relation to geodynamic setting: A DEM-based analysis. J. Volcanol. Geoth. Res. 217, 56–72.

Friedrichs, B., Atıcı, G., Danišík, M., Atakay, E., Çobankaya, M., Harvey, J.C., Yurteri, E., Schmitt, A.K., 2020a. Late Pleistocene eruptive recurrence in the post-collisional Mt. Hasan stratovolcanic complex (Central Anatolia) revealed by zircon double-dating. J. Volcanol. Geoth. Res., 404, 107007.

Friedrichs, B., Atıcı, G., Danišík, M., Yurteri, E., Schmitt, A.K., 2020b. Sequence modeling in zircon double-dating of early Holocene Mt. Erciyes domes (Central Anatolia). Quat. Geochronol. , 61, 101129.

Froger, J.L., Lénat, J.F., Chorowicz, J., Le Pennec, J.L., Bourdier, J.L., Köse, O., Zimitoglu, O., Gündogdu, N., Gourgaud, A., 1998. Hidden calderas evidenced by multisource geophysical data; example of Cappadocian Calderas, Central Anatolia. J. Volcanol. Geoth. Res. 85, 99–128.

Genç, Y., Yürür, M.T., 2010. Coeval extension and compression in Late Mesozoic–Recent thin-skinned extensional tectonics in Central Anatolia, Turkey. J Struct. Geol. 32, 623–640.

Gençalioğlu-Kuşcu, G., 2011. Geochemical characterization of a Quaternary monogenetic volcano in Erciyes volcanic complex: Cora Maar (Central Anatolian volcanic province, Turkey). Int. J. Earth Sci. 100, 1967–1985.

Gençalioğlu-Kuşcu, G., Atilla, C., Cas, R.A., Kuscu, I., 2007. Base surge deposits, eruption history, and depositional processes of a wet phreatomagmatic volcano in Central Anatolia (Cora Maar). J. Volcanol. Geoth. Res. 159, 198–209.

Gençalioğlu-Kuşcu, G., Geneli, F., 2010. Review of post-collisional volcanism in the Central Anatolian Volcanic Province (Turkey), with special reference to the Tepekoy Volcanic Complex. Int. J. Earth Sci. 99, 593–621.

Gençoğlu-Korkmaz, G., Asan, K., Kurt, H., Morgan, G., 2017. 40Ar/39Ar geochronology, elemental and Sr-Nd-Pb isotope geochemistry of the Neogene bimodal volcanism in the Yukselen area, NW Konya (Central Anatolia, Turkey). J. Afr. Earth Sci. 129, 427–444.

Germa, A., Connor, L.J., Cañon-Tapia, E., Le Corvec, N., 2013. Tectonic and magmatic controls on the location of post-subduction monogenetic volcanoes in Baja California, Mexico, revealed through spatial analysis of eruptive vents. Bull. Volcanol. 75, 782.

Gevrek, A.I., Kazancı, N., 2000. A Pleistocene, pyroclastic-poor maar from central Anatolia, Turkey: influence of a local fault on a phreatomagmatic eruption. J. Volcanol. Geoth. Res. 95, 309–317.

Göğüş, O.H., Pysklywec, R.N., Şengör, A., Gün, E., 2017. Drip tectonics and the enigmatic uplift of the Central Anatolian Plateau. Nat. Commun. 8, 1–9.

Gómez-Vasconcelos, M.G., Luis Macías, J., Avellán, D.R., Sosa-Ceballos, G., Garduño-Monroy, V.H., Cisneros-Máximo, G., Layer, P.W., Benowitz, J., López-Loera, H., López, F.M., et al., 2020. The control of preexisting faults on the distribution, morphology, and volume of monogenetic volcanism in the Michoacán-Guanajuato Volcanic Field. Geol. Soc. Am. Bull., 132, 2455–2474 .

Göncüoglu, C., Dirik, K., Erler, A., Yalnız, K., 1994. Orta Anadolu Masifinin dogu bölümünün jeolojisi.

Göncüoğlu, M., Toprak, V., 1992. Neogene and quaternary volcanism of central anatolia: a volcano-structural evaluation. Bulletin de la Section de Volcanologie, Société Géologique de France 26, 1–6.

Grassberger, P., Procaccia, I., 1983. Characterization of strange attractors. Phys. Rev. Lett. 50, 346.

Gudmundsson, A., 2006. How local stresses control magma-chamber ruptures, dyke injections, and eruptions in composite volcanoes. Earth-Sci. Rev. 79, 1–31.

Gudmundsson, A., 2012. Magma chambers: Formation, local stresses, excess pressures, and compartments. J. Volcanol. Geoth. Res. 237, 19–41.

Gudmundsson, A., Brenner, S.L., 2005. On the conditions of sheet injections and eruptions in stratovolcanoes. Bull. Volcanol. 67, 768–782.

Gürbüz, E., Seyitoğlu, G., Güney, A., 2020. Late Cenozoic tectono-sedimentary evolution of the Ulukışla Basin: progressive basin development in south-central Turkey. Int. J. Earth Sci. 109, 345–371.

Gürsoy, H., Piper, J., Tatar, O., 2003. Neotectonic deformation in the western sector of tectonic escape in Anatolia: palaeomagnetic study of the Afyon region, central Turkey. Tectonophysics 374, 57–79.

Gürsoy, H., Piper, J., Tatar, O., Mesci, L., 1998. Palaeomagnetic study of the Karaman and Karapinar volcanic complexes, central Turkey: neotectonic rotation in the south-central sector of the Anatolian Block. Tectonophysics 299, 191–211.

Gutenberg, B., Richter, C.F., 1944. Frequency of earthquakes in California. Bull. Seismol. Soc. Am. 34, 185–188.

Haag, M.B., Baez, W.A., Sommer, C.A., Arnosio, J.M., Filipovich, R.E., 2019. Geomorphology and spatial distribution of monogenetic volcanoes in the southern Puna Plateau (NW Argentina). Geomorphology 342, 196–209.

Hamann, Y., Wulf, S., Ersoy, O., Ehrmann, W., Aydar, E., Schmiedl, G., 2010. First evidence of a distal early Holocene ash layer in Eastern Mediterranean deep-sea sediments derived from the Anatolian volcanic province. Quat. Res. 73, 497–506.

Hamilton, C.W., Fagents, S.A., Thordarson, T., 2010. Explosive lava–water interactions II: self-organization processes among volcanic rootless eruption sites in the 1783–1784 Laki lava flow, Iceland. Bull. Volcanol. 72, 469–485.

Hamilton, H.C., Falconer, W., 1903. The geography of Strabo. volume 1. G. Bell & Sons.

Hasenaka, T., Carmichael, I.S., 1985. The cinder cones of Michoacán—Guanajuato, central Mexico: their age, volume and distribution, and magma discharge rate. J. Volcanol. Geoth. Res. 25, 105–124.

Hentschel, H., Procaccia, I., 1983. The infinite number of generalized dimensions of fractals and strange attractors. Physica. D-Nonlinear Phen. 8, 435–444.

Higgins, M., Schoenbohm, L.M., Brocard, G., Kaymakci, N., Gosse, J.C., Cosca, M.A., 2015. New kinematic and geochronologic evidence for the Quaternary evolution of the Central Anatolian fault zone (CAFZ). Tectonics 34, 2118–2141.

Hirabayashi, T., Ito, K., Yoshii, T., 1992. Multifractal analysis of earthquakes, in: Fractals and Chaos in the Earth Sciences. Springer, pp. 591–610.

Inbar, M., Gilichinsky, M., Melekestsev, I., Melnikov, D., Zaretskaya, N., 2011. Morphometric and morphological development of Holocene cinder cones: a field and remote sensing study in the Tolbachik volcanic field, Kamchatka. J. Volcanol. Geoth. Res. 201, 301–311.

Kaislaniemi, L., Van Hunen, J., Allen, M., Neill, I., 2014. Sublithospheric small-scale convection—a mechanism for collision zone magmatism. Geology 42, 291–294.

Karatson, D., Telbisz, T., Harangi, S., Magyari, E., Dunkl, I., Kiss, B., Janosi, C., Veres, D., Braun, M., Fodor, E., et al., 2013. Morphometrical and geochronological constraints on the youngest eruptive activity in East-Central Europe at the Ciomadul (Csomád) lava dome complex, East Carpathians. J. Volcanol. Geoth. Res. 255, 43–56.

Kazancı, N., Gevrek, A., Varol, B., 1995. Facies changes and high calorific peat formation in a Quaternary maar lake, central Anatolia, Turkey: the possible role of geothermal processes in a closed lacustrine basin. Sediment. Geol. 94, 255–266.

Keller, J., 1974. Quaternary maar volcanism near Karapinar in Central Anatolia. Bull. Volcanol. 38, 378–396.

Kereszturi, G., Adelina, G., Marti, J., Németh, K., Doniz-Paez, F.J., 2013a. Evaluation of morphometry-based dating of monogenetic volcanoes–a case study from Bandes del Sur, Tenerife (Canary Islands). Bull. Volcanol. 75, 734.

Kereszturi, G., Jordan, G., Németh, K., Dóniz-Páez, J.F., 2012. Syn-eruptive morphometric variability of monogenetic scoria cones. Bull. Volcanol. 74, 2171–2185.

Kereszturi, G., Németh, K., 2012a. Monogenetic basaltic volcanoes: genetic classification, growth, geomorphology and degradation, in: Updates in volcanology-new advances in understanding volcanic systems. IntechOpen.

Kereszturi, G., Németh, K., Cronin, S.J., Agustín-Flores, J., Smith, I.E., Lindsay, J., 2013b. A model for calculating eruptive volumes for monogenetic volcanoes—Implication for the Quaternary Auckland Volcanic Field, New Zealand. J. Volcanol. Geoth. Res. 266, 16–33.

Kereszturi, G., Németh, K., K, 2012b. Structural and morphometric irregularities of eroded Pliocene scoria cones at the Bakony-Balaton Highland Volcanic Field, Hungary. Geomorphology 136, 45–58.

Kervyn, M., Ernst, G., Carracedo, J.C., Jacobs, P., 2012. Geomorphometric variability of "monogenetic" volcanic cones: evidence from Mauna Kea, Lanzarote and experimental cones. Geomorphology 136, 59–75.

Kocaarslan, A., Ersoy, E.Y., 2018. Petrologic evolution of Miocene-Pliocene mafic volcanism in the Kangal and Gürün basins (Sivas-Malatya), central east Anatolia: Evidence for Miocene anorogenic magmas contaminated by continental crust. Lithos 310, 392–408.

Koçyiğit, A., Beyhan, A., 1998. A new intracontinental transcurrent structure: the Central Anatolian Fault Zone, Turkey. Tectonophysics 284, 317–336.

Koçyiğit, A., Erol, O., 2001. A tectonic escape structure: Erciyes pull-apart basin, Kayseri, central Anatolia, Turkey. Geol. Acta 14, 133–145.

Kósik, S., Bebbington, M., Németh, K., 2020. Spatio-temporal hazard estimation in the central silicic part of Taupo Volcanic Zone, New Zealand, based on small to medium volume eruptions. Bull. Volcanol. 82, 50.

Krystopowicz, N.J., Schoenbohm, L.M., Rimando, J., Brocard, G., Rojay, B., 2020. Tectonic geomorphology and Plio-Quaternary structural evolution of the Tuzgölü fault zone, Turkey: Implications for deformation in the interior of the Central Anatolian Plateau. Geosphere, 16, 1107–1124.

Kurokawal, K., Otsukil, K., Hasenaka, T., 1995. Michoacán-Guanajuato region of the Mexican Volcanic Belt. Geofis. Int. 34, 309–320.

Kuzucuoğlu, C., Atakay, E.G., Mouralis, D., Atıcı, G., Guillou, H., Türkecan, A., Pastre, J.F., 2020. Geomorphology and tephrochronology review of the Hasandağ volcano (southern Cappadocia, Turkey). Mediterr. Sci. Rev. , 2, 1–31.

Kuzucuoğlu, C., Bertaux, J., Black, S., Denefle, M., Fontugne, M., Karabiyikoğlu, M., Kashima, K., Limondin-Lozouet, N., Mouralis, D., Orth, P., 1999. Reconstruction of climatic changes during the Late Pleistocene, based on sediment records from the Konya Basin (Central Anatolia, Turkey). Geol. J. 34, 175–198.

Le Corvec, N., McGovern, P.J., Grosfils, E.B., Galgana, G., 2015. Effects of crustal-scale mechanical layering on magma chamber failure and magma propagation within the Venusian lithosphere. J. Geophys. Res. Planets 120, 1279–1297.

Le Corvec, N., Menand, T., Lindsay, J., 2013b. Interaction of ascending magma with pre-existing crustal fractures in monogenetic basaltic volcanism: an experimental approach. J. Geophys. Res-Sol. Ea. 118, 968–984.

Le Corvec, N., Spörli, K.B., Rowland, J., Lindsay, J., 2013a. Spatial distribution and alignments of volcanic centers: clues to the formation of monogenetic volcanic fields. Earth-Sci. Rev. 124, 96–114.

Le Pennec, J.L., Bourdier, J.L., Froger, J.L., Temel, A., Camus, G., Gourgaud, A., 1994. Neogene ignimbrites of the Nevsehir plateau (central Turkey): stratigraphy, distribution and source constraints. J. Volcanol. Geoth. Res. 63, 59–87.

Legrand, D., 2002. Fractal dimensions of small, intermediate, and large earthquakes. Bull. Seismol. Soc. Am. 92, 3318–3320.

Lorenz, V., 1975. Formation of phreatomagmatic maar–diatreme volcanoes and its relevance to kimberlite diatremes, in: Physics and Chemistry of the Earth. Elsevier, pp. 17–27.

Lutz, T.M., 1986. An analysis of the orientations of large-scale crustal structures: A statistical approach based on areal distributions of pointlike features. J. Geophys. Res-Sol. Ea. 91, 421–434.

Malamud, B.D., Turcotte, D.L., 1999. Self-organized criticality applied to Nat. Hazards. Nat. Hazards 20, 93–116.

Malamud, B.D., Turcotte, D.L., 2006. The applicability of power-law frequency statistics to floods. J. Hydrol. 322, 168–180.

Mandelbrot, B.B., 1975. Les objets fractals: forme, hasard et dimension. Flammarion, 212 p.

Marliyani, G.I., Helmi, H., Arrowsmith, J.R., Clarke, A., 2020. Volcano morphology as an indicator of stress orientation in the Java Volcanic Arc, Indonesia. J. Volcanol. Geoth. Res. , 106912.

Mazzarini, F., 2004. Volcanic vent self-similar clustering and crustal thickness in the northern Main Ethiopian Rift. Geophys. Res. Lett. 31, L04604.

Mazzarini, F., 2007. Vent distribution and crustal thickness in stretched continental crust: The case of the Afar Depression (Ethiopia). Geosphere 3, 152–162.

Mazzarini, F., Armienti, P., 2001. Flank cones at Mount Etna Volcano: do they have a power-law distribution? Bull. Volcanol. 62, 420–430.

Mazzarini, F., D'Orazio, M., 2003. Spatial distribution of cones and satellite-detected lineaments in the Pali Aike Volcanic Field (southernmost Patagonia): insights into the tectonic setting of a Neogene rift system. J. Volcanol. Geoth. Res. 125, 291–305.

Mazzarini, F., Ferrari, L., Isola, I., 2010. Self-similar clustering of cinder cones and crust thickness in the Michoacan–Guanajuato and Sierra de Chichinautzin volcanic fields, Trans-Mexican Volcanic Belt. Tectonophysics 486, 55–64.

Mazzarini, F., Isola, I., 2010. Monogenetic vent self-similar clustering in extending continental crust: Examples from the East African Rift System. Geosphere 6, 567–582.

Mazzarini, F., Keir, D., Isola, I., 2013. Spatial relationship between earthquakes and volcanic vents in the central-northern Main Ethiopian Rift. J. Volcanol. Geoth. Res. 262, 123–133.

Mazzarini, F., Le Corvec, N., Isola, I., Favalli, M., 2016. Volcanic field elongation, vent distribution, and tectonic evolution of a continental rift: The Main Ethiopian Rift example. Geosphere 12, 706–720.

Mouralis, D., Pastre, J.F., Kuzucuoglu, C., Türkecan, A., Atici, Y., Slimak, L., Guillou, H., Kunesch, S., 2002. Les complexes volcaniques Rhyolithiques quaternaires d'Anatolie centrale (Göllü Dag et Acigöl, Turquie): Genèse, instabilité, contraintes environnementales. Quaternaire 13, 219–228.

Muirhead, J.D., Airoldi, G., Rowland, J.V., White, J.D., 2012. Interconnected sills and inclined sheet intrusions control shallow magma transport in the Ferrar large igneous province, Antarctica. Geol. Soc. Am. Bull. 124, 162–180.

Muirhead, J.D., Kattenhorn, S.A., Le Corvec, N., 2015. Varying styles of magmatic strain accommodation across the E ast A frican Rift. Geochem. Geophys. Geosyst. 16, 2775–2795.

Muller, J.R., Ito, G., Martel, S.J., 2001. Effects of volcano loading on dike propagation in an elastic half-space. J. Geophys. Res-Sol. Ea. 106, 11101–11113.

Murcia, H., Borrero, C., Németh, K., 2019. Overview and plumbing system implications of monogenetic volcanism in the northernmost Andes' volcanic province. J. Volcanol. Geoth. Res. 383, 77–87.

Nakamura, K., 1977. Volcanoes as possible indicators of tectonic stress orientation—principle and proposal. J. Volcanol. Geoth. Res. 2, 1–16.

Nakamura, K., Jacob, K.H., Davies, J.N., 1977. Volcanoes as possible indicators of tectonic stress orientation—Aleutians and Alaska, in: Stress in the Earth. Springer, pp. 87–112.

Németh, K., 2010. Monogenetic volcanic fields: Origin, sedimentary record, and relationship with polygenetic volcanism. What is a Volcano? 470, 43.

Németh, K., Kereszturi, G., 2015. Monogenetic volcanism: personal views and discussion. Int. J. Earth Sci. 104, 2131–2146.

Németh, K., Kósik, S., 2020. Review of Explosive Hydrovolcanism. Geosciences 10, 44.

Németh, K., Risso, C., Nullo, F., Kereszturi, G., 2011. The role of collapsing and cone rafting on eruption style changes and final cone morphology: Los Morados scoria cone, Mendoza, Argentina. Central European Journal of Geosciences 3, 102–118.

Notsu, K., Fujitani, T., Ui, T., Matsuda, J., Ercan, T., 1995. Geochemical features of collision-related volcanic rocks in central and eastern Anatolia, Turkey. J. Volcanol. Geoth. Res. 64, 171–191.

Okay, A.I., Tüysüz, O., 1999. Tethyan sutures of northern Turkey. (Geol. Soc. Spec. Publ. 156, 475–515.

Okay, A.I., Zattin, M., Cavazza, W., 2010. Apatite fission-track data for the Miocene Arabia-Eurasia collision. Geology 38, 35–38.

Özsayın, E., Çiner, A., Rojay, B., Dirik, K., Melnick, D., Fernandez-Blanco, D., Bertotti, G., Schildgen, T.F., Garcin, Y., Strecker, M.R., et al., 2013. Plio-Quaternary extensional tectonics of the Central Anatolian Plateau: a case study from the Tuz Gölü Basin, Turkey. Turk. J. Earth Sci. 22, 691–714.

Pasquare, G., Poli, S., Vezzoli, L., Zanchi, A., 1988. Continental arc volcanism and tectonic setting in Central Anatolia, Turkey. Tectonophysics 146, 217–230.

Paulsen, T.S., Wilson, T.J., 2009. Structure and age of volcanic fissures on Mount Morning: A new constraint on Neogene to contemporary stress in the West Antarctic Rift, southern Victoria Land, Antarctica. Geol. Soc. Am. Bull. 121, 1071–1088.

Paulsen, T.S., Wilson, T.J., 2010. New criteria for systematic mapping and reliability assessment of monogenetic volcanic vent alignments and elongate volcanic vents for crustal stress analyses. Tectonophysics 482, 16–28.

Pearce, J.A., Baker, P.E., Harvey, P.K., Luff, I.W., 1995. Geochemical evidence for subduction fluxes, mantle melting and fractional crystallization beneath the South Sandwich island arc. J. Petrol. 36, 1073–1109.

Pérez-López, R., Legrand, D., Garduño-Monroy, V., Rodríguez-Pascua, M., Giner-Robles, J., 2011. Scaling laws of the size-distribution of monogenetic volcanoes within the Michoacán-Guanajuato Volcanic Field (Mexico). J. Volcanol. Geoth. Res. 201, 65–72.

Philippon, M., Brun, J.P., Gueydan, F., Sokoutis, D., 2014. The interaction between Aegean back-arc extension and Anatolia escape since Middle Miocene. Tectonophysics 631, 176–188.

Piper, J., Gürsoy, H., Tatar, O., 2002. Palaeomagnetism and magnetic properties of the Cappadocian ignimbrite succession, central Turkey and Neogene tectonics of the Anatolian collage. J. Volcanol. Geoth. Res. 117, 237–262.

Platzman, E., Tapirdamaz, C., Sanver, M., 1998. Neogene anticlockwise rotation of central Anatolia (Turkey): preliminary palaeomagnetic and geochronological results. Tectonophysics 299, 175–189.

Pollard, D.D., Aydin, A., 1984. Propagation and linkage of oceanic ridge segments. J. Geophys. Res-Sol. Ea. 89, 10017–10028.

Porter, S.C., 1972. Distribution, morphology, and size frequency of cinder cones on Mauna Kea volcano, Hawaii. Geol. Soc. Am. Bull. 83, 3607–3612.

Pourteau, A., Sudo, M., Candan, O., Lanari, P., Vidal, O., Oberhänsli, R., 2013. Neotethys closure history of Anatolia: insights from 40Ar–39Ar geochronology and P–T estimation in high-pressure metasedimentary rocks. Journal of Metamorphic Geology 31, 585–606.

Prima, O.D.A., Yoshida, T., 2010. Characterization of volcanic geomorphology and geology by slope and topographic openness. Geomorphology 118, 22–32.

Rabayrol, F., Hart, C.J., Thorkelson, D.J., 2019. Temporal, spatial and geochemical evolution of late Cenozoic post-subduction magmatism in central and eastern Anatolia, Turkey. Lithos 336, 67–96.

Reid, M., Delph, J., Cosca, M., Schleiffarth, W., Gençalioğlu-Kuş, G., 2019. Melt equilibration depths as sensors of lithospheric thickness during Eurasia-Arabia collision and the uplift of the Anatolian Plateau. Geology 47, 943–947.

Reid, M.R., Schleiffarth, W.K., Cosca, M.A., Delph, J.R., Blichert-Toft, J., Cooper, K.M., 2017. Shallow melting of MORB-like mantle under hot continental lithosphere, Central Anatolia. Geochem. Geophys. Geosyst. 18, 1866–1888.

Riedel, C., Ernst, G., Riley, M., 2003. Controls on the growth and geometry of pyroclastic constructs. J. Volcanol. Geoth. Res. 127, 121–152.

Roberts, N., Reed, J., Leng, M., Kuzucuoğlu, C., Fontugne, M., Bertaux, J., Woldring, H., Bottema, S., Black, S., Hunt, E., et al., 2001. The tempo of Holocene climatic change in the eastern Mediterranean region: new high-resolution crater-lake sediment data from central Turkey. The Holocene 11, 721–736.

Rodriguez-Gonzalez, A., Fernandez-Turiel, J., Perez-Torrado, F.J., Gimeno, D., Aulinas, M., 2010. Geomorphological reconstruction and morphometric modelling applied to past volcanism. Int. J. Earth Sci. 99, 645–660.

Sanders, J., 2008. Veusz-a scientific plotting package.

Sarıkaya, M.A., Çiner, A., Zreda, M., Şen, E., Ersoy, O., 2019. Chlorine degassing constrained by cosmogenic 36Cl and radiocarbon dating of early Holocene rhyodacitic lava domes on Erciyes stratovolcano, central Turkey. J. Volcanol. Geoth. Res. 369, 263–275.

Sato, H., Taniguchi, H., 1997. Relationship between crater size and ejecta volume of recent magmatic and phreato-magmatic eruptions: Implications for energy partitioning. Geophys. Res. Lett 24, 205–208.

Schildgen, T.F., Yıldırım, C., Cosentino, D., Strecker, M.R., 2014. Linking slab breakoff, Hellenic trench retreat, and uplift of the Central and Eastern Anatolian plateaus. Earth-Sci. Rev. 128, 147–168.

Schleiffarth, W., Darin, M., Reid, M., Umhoefer, P.J., 2018. Dynamics of episodic Late Cretaceous–Cenozoic magmatism across Central to Eastern Anatolia: New insights from an extensive geochronology compilation. Geosphere 14, 1990–2008.

Schmitt, A.K., Danisik, M., Aydar, E., Şen, E., Ulusoy, I., Lovera, O.M., 2014. Identifying the volcanic eruption depicted in a neolithic painting at Catalhoyuk, Central Anatolia, Turkey. PLoS One 9.

Schmitt, A.K., Danišík, M., Evans, N.J., Siebel, W., Kiemele, E., Aydin, F., Harvey, J.C., 2011. Acigöl rhyolite field, Central Anatolia (part 1): high-resolution dating of eruption episodes and zircon growth rates. Contrib. Mineral. Petrol. 162, 1215–1231.

Settle, M., 1979. The structure and emplacement of cinder cone fields. Am. J. Sci. 279, 1089–1107.

Siebel, W., Schmitt, A.K., Kiemele, E., Danišík, M., Aydin, F., 2011. Acigöl rhyolite field, central Anatolia (part II): geochemical and isotopic (Sr–Nd–Pb, δ 18 O) constraints on volcanism involving two high-silica rhyolite suites. Contrib. Mineral. Petrol. 162, 1233–1247.

Şen, E., 1997. Erciyes Stratovolkanı'nın (Orta Anadolu) volkanolojik ve petrolojik gelişiminin incelenmesi. Master's thesis. Hacettepe University, Ankara, 268p.

Şen, E., Aydar, E., Bayhan, H., Gourgaud, A., 2014. Alkali Bazalt ve Piroklastik Çökellerin Volkanolojik Özellikleri, Kula Volkanları, Batı Anadolu Volcanological Characteristics of Alkaline Basalt and Pyroclastic Deposits, Kula Volcanoes, Western Anatolia. Bull. Earth Sci. App. Res. Cent. Hacettepe Univ. 35, 219–252.

Şen, E., Aydar, E., Gourgaud, A., Kurkcuoglu, B., 2002. La phase explosive précédant l'extrusion des dômes volcaniques: exemple du dôme rhyodacitique de Dikkartin Dag, Erciyes, Anatolie centrale, Turquie. Comptes Rendus Geoscience 334, 27–33.

Şen, E., Kürkçüoğlu, B., Aydar, E., Gourgaud, A., Vincent, P.M., 2003. Volcanological evolution of Mount Erciyes stratovolcano and origin of the Valibaba Tepe ignimbrite (Central Anatolia, Turkey). J. Volcanol. Geoth. Res. 125, 225–246.

Şengör, A., Görür, N., Şaroğlu, F., 1985. Strike-slip faulting and related basin formation in zones of tectonic escape: Turkey as a case study, in: Strike-slip deformation, basin formation and sedimentation. Spec. Pub. SEPM. volume 37, pp. 227–264.

Tadono, T., Takaku, J., Tsutsui, K., Oda, F., Nagai, H., 2015. Status of "ALOS World 3D (AW3D)" global DSM generation, in: 2015 IEEE International Geoscience and Remote Sensing Symposium (IGARSS), IEEE. pp. 3822–3825.

Takada, A., 1994. The influence of regional stress and magmatic input on styles of monogenetic and polygenetic volcanism. J. Geophys. Res-Sol. Ea. 99, 13563–13573.

Tank, S.B., Karaş, M., 2020. Unraveling the electrical conductivity structure to decipher the hydrothermal system beneath the Mt. Hasan composite volcano and its vicinity, SW Cappadocia, Turkey. J. Volcanol. Geoth. Res. , 107048.

Tatar, O., Piper, J.D., Gürsoy, H., 2000. Palaeomagnetic study of the Erciyes sector of the Ecemiş Fault Zone: neotectonic deformation in the southeastern part of the Anatolian Block. Geol. Soc. Spec. Publ. 173, 423–440.

Tibaldi, A., 1995. Morphology of pyroclastic cones and tectonics. J. Geophys. Res-Sol. Ea. 100, 24521–24535.

Tokçaer, M., Agostini, S., Savascin, M., 2005. Geotectonic setting and origin of the youngest Kula volcanics (western Anatolia), with a new emplacement model. Turk. J. Earth. Sci. 14(2), 145–166.

Toprak, V., 1998. Vent distribution and its relation to regional tectonics, Cappadocian Volcanics, Turkey. J. Volcanol. Geoth. Res. 85, 55–67.

Toprak, V., Göncüoglu, M., 1993. Tectonic control on the development of the neogene-quaternary central anatolian volcanic province, Turkey. Geol. J. 28, 357–369.

Toprak, V., Kaymakçı, N., 1995. Determination of Stress Orientation Using Slip Lineation Data in Pliocene Ignimbrites Around Derinkuyu Fault (Nevşehir). Turk. J. Earth. Sci. 4, 39–47.

Tuncer, A., Tunoğlu, C., Aydar, E., Yilmaz, I.O., Gümüş, B.A., Şen, E., 2019. Holocene paleoenvironmental evolution of the Acıgöl paleo maar lake (Nevşehir, Central Anatolia). Med. Geo. Rev. 1, 255–269.

Turcotte, D., Greene, L., 1993. A scale-invariant approach to flood-frequency analysis. Stoch. Hydrol. Hydraul. 7, 33–40.

Türkecan, A., Kuzucuoğlu, C., Mouralis, D., Pastre, J., Atıcı, Y., Guillou, H., Fontugne, M., 2004. Upper Pleistocene volcanism and palaeogeography in Cappadocia, Turkey. Technical Report. TÜBİTAK Project No.101Y109, MTA Report No.10652.

Tveite, H., 2015–2020. The QGIS Line Direction Histogram Plugin, howpublished = http://plugins.qgis.org/plugins/linedirectionhistogram/.

Ulusoy, I., Labazuy, P., Aydar, E., Atak, O., Yürür, T., Artuner, H., Dahlin, T., 2009. Multisource geophysical investigation of the Acıgöl caldera structure (central Turkey): preliminary results, in: EGU General Assembly Conference Abstracts, p. 7746.

Unglert, K., Radić, V., Jellinek, A.M., 2016. Principal component analysis vs. self-organizing maps combined with hierarchical clustering for pattern recognition in volcano seismic spectra. J. Volcanol. Geoth. Res. 320, 58–74.

Uslular, G., Gençalioğlu-Kuşcu, G., 2019a. Geochemical characteristics of Anatolian basalts: Comment on "Neogene uplift and magmatism of Anatolia: Insights from drainage analysis and basaltic geochemistry" by McNab et al. Geochem. Geophys. Geosyst. 20, 530–541.

Uslular, G., Gençalioğlu-Kuşcu, G., 2019b. Mantle source heterogeneity in monogenetic basaltic systems: A case study of Eğrikuyu monogenetic field (Central Anatolia, Turkey). Geosphere 15, 295–323.

Uslular, G., Gençalioğlu-Kuşcu, G., 2020. Orta Anadolu Maarlarının insansız Hava Araçları (iHA) Kullanılarak 3B Modellenmesi ve Morfolojik, Fiziksel ve Jeokimyasal Özelliklerinin Karşılaştırılması. Technical Report. no. 118Y360 TÜBİTAK 1002, 191 s, in Turkish (with English Abstract).

Uslular, G., Gençalioğlu-Kuşcu, G., Arcasoy, A., 2015. Size-distribution of scoria cones within the Eğrikuyu monogenetic field (Central Anatolia, Turkey). J. Volcanol. Geoth. Res. 301, 56–65.

Valentine, G.A., Krogh, K.E., 2006. Emplacement of shallow dikes and sills beneath a small basaltic volcanic center–The role of pre-existing structure (Paiute Ridge, southern Nevada, USA). Earth Planet. Sc. Lett. 246, 217–230.

Vanacore, E., Taymaz, T., Saygin, E., 2013. Moho structure of the Anatolian Plate from receiver function analysis. Geophys. J. Int. 193, 329–337.

van den Hove, J., Grose, L., Betts, P.G., Ailleres, L., Van Otterloo, J., Cas, R.A., 2017. Spatial analysis of an intra-plate basaltic volcanic field in a compressional tectonic setting: South-eastern Australia. J. Volcanol. Geoth. Res. 335, 35–53.

Van Wyk de Vries, B., Merle, O., 1998. Extension induced by volcanic loading in regional strike-slip zones. Geology 26, 983–986.

Wadge, G., Cross, A., 1988. Quantitative methods for detecting aligned points: An application to the volcanic vents of the Michoacan-Guanajuato volcanic field, Mexico. Geology 16, 815–818.

Wilson, M., Tankut, A., Guleç, N., 1997. Tertiary volcanism of the Galatia province, north-west Central Anatolia, Turkey. Lithos 42, 105–121.

Wood, C.A., 1980. Morphometric analysis of cinder cone degradation. J. Volcanol. Geoth. Res. 8, 137–160.

Yıldırım, T., Özgür, R., 1981. Acıgöl kalderası. Jeo. Derg. 10, 59–70.

Table 1: Summary of Quaternary Monogenetic Clusters in the CAVP (modified after Toprak, 1998). Age data are restricted to those directly related to monogenetic edifices, otherwise not considered.

Cluster Name	**Edifice**	**Composition**	**Age (Ma)**	**Method**	**Alignment**
EVC	Lava Dome (100)	dacitic to rhyolitic	0.008-0.60	U-Th/He^{a} ^{36}Cl^{b} Ar-Ar^{c}	radial with a dominant NE-SW trend
	Scoria Cone (40)	basaltic to andesitic	0.01-0.71	K-Ar^{d}	
	Maar (1)	basaltic andesitic	0.13-0.35	K-Ar^{e}	
	Undif. (44)				
NAVC	Lava Dome (24)	andesitic to rhyolitic	0.02-0.17	U-Th/He^{f} K-Ar^{g}	N-S NW-SE
	Scoria Cone (10)	basaltic to andesitic	0.03-0.62	K-Ar^{g}	
	Maar (6)*	rhyolitic	0.02	U-Th/He^{f}	
	Tuff Ring (2)*	basaltic	0.08-0.11	K-Ar^{g}	
	Undif. (28)				
DVC	Lava Dome (30)	dacitic to rhyolitic	0.09-1.10	U-Pb^{h} K-Ar^{g}	N-S NE-SW
	Scoria Cone (28)	basaltic to basaltic andesite	0.15-0.49	Ar-Ar^{h,i} K-Ar^{g}	
	Maar (1)	basaltic			
	Undif. (3)				
HKVC	Lava Dome (11)	andesitic to rhyolitic	0.009-0.70	U-Th/He^{j,k} Ar-Ar^{h,i}	NW-SE NE-SW
	Scoria Cone (33)	basaltic	0.02-0.13	U-Pb^{h} Ar-Ar^{i,l} K-Ar^{d,m,n}	
	Maar (1)	basaltic			
	Undif. (34)				
EMF	Scoria Cone (110)	basaltic	0.07-2.60	Ar-Ar^{i} K-Ar^{d,m}	N-S NE-SW
	Maar (8)	basaltic	1.30	Ar-Ar^{i}	NW-SE
	Tuff Ring ? (1)	basaltic			
KMF	Scoria Cone (17)	basaltic	0.16-0.50	Ar-Ar^{i} K-Ar^{m}	NE-SW
	Lava Dome (1)	andesitic			
	Maar (4)*	basaltic			
	Undif. (3)				

*including explosion craters; a—Friedrichs et al. (2020b); b—Sarıkaya et al. (2019); c—Higgins et al. (2015); d—Doğan-Külahçı et al. (2018); e—Gençalioğlu-Kuşcu (2011); f—Schmitt et al. (2011); g—Türkecan et al. (2004); h—Aydin et al. (2014); i—Reid et al. (2017); j—Friedrichs et al. (2020a); k—Schmitt et al. (2014); l—Aydar and Gourgaud (1998) and references therein; m—Notsu et al. (1995); n—Kuzucuoğlu et al. (2020)

Table 2: Morphometric parameters of scoria cones within the CAVP

Parameters	Symbol	EVC	NAVC	DVC	HKVC	EMF	KMF
N. of cones	171/238	32	6	22	27	74	10
Cone height (m)	H_{co}	93±8	58±10	75±10	67±10	66±5	77±22
Base diameter (m)	W_{co}	696±46	594±110	690±67	583±66	671±35	606±148
Crater diameter (m)	W_{cr}	195±18	209±101	238±37	205±28	178±12	361±45
Crater depth (m)	H_{cr}	26±3	12±4	27±5	21±4	14±1	43±5
Cone slope (°)	S_{mean}	17.4±0.7	13.0±0.8	13.7±0.9	14.4±0.7	12.3±0.4	16.9±1.5
Volume (m^3)[a]	V_{co}	3.3±0.7E+07	1.8±0.8E+07	2.8±0.8E+07	2.8±0.9E+07	2.5±0.5E+07	3.4±2.0E+07
DRE corrected vol.[b]	V_{DRE}	6.7±1.4E+06	3.7±1.6E+06	5.5±1.7E+06	5.7±1.8E+06	5.1±0.1E+06	6.9±4.0E+06
Ejecta volume (m^3)[c]	V_{ejc}	5.9±1.5E+08	5.7±3.2E+08	4.0±1.2E+08	5.3±1.8+E08	5.6±1.1E+08	2.1±0.4E+08
Total volume (m^3)	V_T	6.0±1.5E+08	5.8±3.3E+08	4.0±1.2E+08	5.4±1.8E+08	5.7±1.1E+08	2.2±0.4E+08
Steep-sided-ness (S)[d]	$2H_{co}/(W_{co}$-$W_{cr})$	0.31±0.02	0.22±0.01	0.26±0.02	0.25±0.01	0.22±0.01	0.29±0.03
Error in S[d]	†	0.08±0.01	0.08±0.01	0.08±0.01	0.10±0.01	0.07±0.01	0.11±0.01
Flat-topped-ness (F)[d]	W_{cr}/W_{co}	0.27±0.02	0.28±0.06	0.31±0.02	0.29±0.02	0.23±0.01	0.37±0.07
Error in F[d]	‡	0.05±0.01	0.06±0.02	0.05±0.01	0.06±0.01	0.05±0.01	0.05±0.01
Relative crater depth[d]	H_{cr}/H_{co}	0.35±0.07	0.18±0.01	0.32±0.04	0.27±0.05	0.20±0.02	0.55±0.26
Crater slope[d]	$2D_{cr}/(W_{cr}$-$W_v)$	0.27±0.04	0.12±0.02	0.21±0.03	0.19±0.02	0.15±0.01	0.26±0.07
Elongation	$W_{co_{min}}/W_{co_{max}}$	Co: 0.78±0.08 Cr: 0.84±0.20	Co: 0.75±0.09 Cr: 0.78±0.31	Co: 0.78±0.08 Cr: 0.84±0.20	Co: 0.79±0.11 Cr: 0.89±0.32	Co: 0.82±0.09 Cr: 0.86±0.41	Co: 0.80±0.12 Cr: 0.83±0.15

[a] Hasenaka and Carmichael (1985), $V_c = \pi H_{co}/12 \times (W_{cr}^2 + W_{cr}W_{co} + W_{co}^2)$

[b] Kereszturi et al. (2013b), $V_{DRE} = V_c \times 0.4 \times 0.5$

[c] Sato and Taniguchi (1997), $W_{cr} = 0.11 \times V_{ejc}^{0.42}$

[d] Bemis and Ferencz (2017)

† $0.5[(2H_{co}+errH)/(W_{co}-W_{cr}-errW)-(2H_{co}-errH)/(W_{co}-W_{cr}+errW)]$

‡ $0.5[(W_{cr}+errW)/(W_{co}-errW)-(W_{cr}-errW)/(W_{co}+errW)]$

Table 3: The average morphometric parameters of lava domes within the CAVP

Parameters	Symbol	EVC	NAVC	DVC	HKVC
N. of domes	91/165	56	13	11	11
Dome height (m)	H_{do}	156±14	152±23	174±22	110±21
Base diameter (m)	W_{do}	857±72	1160±100	1443±176	719±86
Crater diameter (m)	W_{cr}	215±29	316±117	501±288	150±34
Crater depth (m)	H_{cr}	18±2	27±9	47±34	17±7
Dome slope (°)	S_{mean}	20.7±0.6	16.6±1.3	15.2±0.9	19.7±2.4
Volume (m^3)[a]	V_d	8.1±2.0E+07	8.0±2.4E+07	1.7±0.9E+07	2.2±0.7E+07
DRE corrected vol.[b]	V_{DRE}	1.6±0.4E+07	1.6±0.5E+07	3.4±1.8E+07	4.4±1.4E+06
Ejecta volume (m^3)[c]	V_{ejc}	9.8±3.1E+07	1.6±0.8E+08	5.2±4.5+08	2.5±1.0+E07
Total volume (m^3)	V_T	4.3±1.3E+08	6.6±3.1E+07	1.3±1.1E+08	1.4±0.6E+07
Steep-sided-ness (S)[d]	$2H_{co}/(W_{co}\text{-}W_{cr})$	0.38±0.01	0.28±0.02	0.26±0.02	0.35±0.05
Error in S[d]	†	0.07±0.01	0.04±0.01	0.03±0.01	0.08±0.01
Flat-topped-ness (F)[d]	W_{cr}/W_{co}	0.20±0.03	0.26±0.10	021±0.06	0.23±0.05
Error in F[d]	‡	0.04±0.01	0.03±0.01	0.02±0.01	0.06±0.01
Relative crater depth[d]	H_{cr}/H_{co}	0.12±0.03	0.20±0.07	0.15±0.07	0.17±0.11
Crater slope[d]	$2D_{cr}/(W_{cr}\text{-}W_v)$	0.18±0.02	0.19±0.03	0.17±0.04	0.20±0.05
Elongation	$W_{co_{min}}/W_{co_{max}}$	Do: 0.78±0.08 Cr: 0.84±0.20	Do: 0.75±0.09 Cr: 0.78±0.31	Do: 0.78±0.08 Cr: 0.84±0.20	Do: 0.79±0.11 Cr: 0.89±0.32

[a]modified after Hasenaka and Carmichael (1985), $V_d = \pi H_{do}/12 \text{ x } (W_{cr}^2 + W_{cr}W_{do} + W_{do}^2)$

[b]Kereszturi et al. (2013b), $V_{DRE} = V_d \text{ x } 0.4 \text{ x } 0.5$

[c]Sato and Taniguchi (1997), $W_{cr} = 0.11 \text{ x } V_{ejc}^{0.42}$

[d]modified after Bemis and Ferencz (2017)

† $0.5[(2H_{do}+errH)/(W_{do}\text{-}W_{cr}\text{-}errW)\text{-}(2H_{do}\text{-}errH)/(W_{do}\text{-}W_{cr}+errW)]$

‡ $0.5[(W_{cr}+errW)/(W_{do}\text{-}errW)\text{-}(W_{cr}\text{-}errW)/(W_{do}+errW)]$

Table 4: The parameters of vent spacing and self-similar clustering

Cluster	**N**	**s (m)**	**CV**	**c**	***Df***	**L_{co} (km)**	**U_{co} (km)**	**R^2**
EVC	185	939	1.15	2 x 10E-07	1.55	0.8	10.0	0.99
NAVC	76	945	1.19	1 x 10E-05	1.16	0.8	12.0	0.99
DVC	62	1676	0.81	4 x 10E-08	1.80	0.6	8.5	0.99
HKVC	79	1212	1.42	-	-	-	-	-
EMF	118	1138	0.96	3 x 10E-07	1.48	0.5	16.0	0.99
KMF	25	1131	0.97	-	-	-	-	-
Vent Type								
Scoria Cone	238	-	-	2 x 10E-07	1.40	0.5	15.0	0.99
Lava Dome	165	-	-	4 x 10E-06	1.13	0.7	8.0	0.99

N: number of vents; s: average vent separation; CV: coefficient of variation; c: normalization constant; *Df*: fractal exponent (D_2); L_{co}: lower cut-off; U_{co}: upper cut-off; R^2: coefficient of correlation

Table 5: The results of the PNN and vent alignment analysis for each monogenetic cluster in the CAVP

	Basic parameters	**EVC**	**NAVC**	**DVC**	**HKVC**	**EMF**	**KMF**
Measured NN parameters	Area Convex Hull (m^2)	8.68E+08	3.10E+08	4.59E+08	8.55E+08	8.11E+08	1.2E+08
	Density (vent/m^2)	2.13E-07	2.39E-07	1.18E-07	0.91E-07	1.45E-07	2.05E-07
	Mean distance NN (m)	939	945	1676	1212	1138	1131
	Expected mean distance NN (m)	1083	1023	1739	1692	1311	1104
	Skewness	6.56	2.96	1.45	3.66	5.22	1.79
	Kurtosis	64.39	10.08	2.07	14.67	40.71	2.58
NN results relative to the Poisson model	R	0.87	0.94	0.96	0.71	0.87	1.03
	Distribution	Clustered	Poisson	Poisson	Clustered	Clustered	Poisson
	C	-3.46	-1.02	-0.60	-4.9	-2.74	0.92
	Model fit	Rejected	Significant	Significant	Rejected	Rejected	Significant
Alignment Analysis	Best max. distance (m)	1360	1552	5118	2606	3738	3291
	N. of alignments	26	29	12	49	28	7
	Artifact %	12	9.4	0	10	9.7	0
Shape Analysis	Short axis ellipse (m)	29,850	19,209	28,743	22,897	29,918	14,809
	Long axis ellipse (m)	37,202	27,707	31,780	51,705	49,882	15,856
	Short axis / Long axis	0.80	0.70	0.90	0.44	0.60	0.93

Table 6: VVD and PCA analysis of monogenetic clusters in the CAVP

Cluster	$\Delta\alpha(°)$	$\alpha(°)$	**ecc**	**Max axis (km)**	**Min axis (km)**
EVC	125	7	0.03	31	29
NAVC	85	125	0.08	21	18
DVC	60	43	0.20	30	20
HKVC	100	74	0.28	40	23
EMF	65	71	0.22	42	26
KMF	70	75	0.13	17	13

$\Delta\alpha(°)$: azimuthal angular dispersion in the VVD histogram; $\alpha(°)$ azimuth of maximum axis of PCA ellipse; ecc: eccentricity of PCA ellipse; Max & Min axis: length of maximum and minimum axis of PCA ellipse

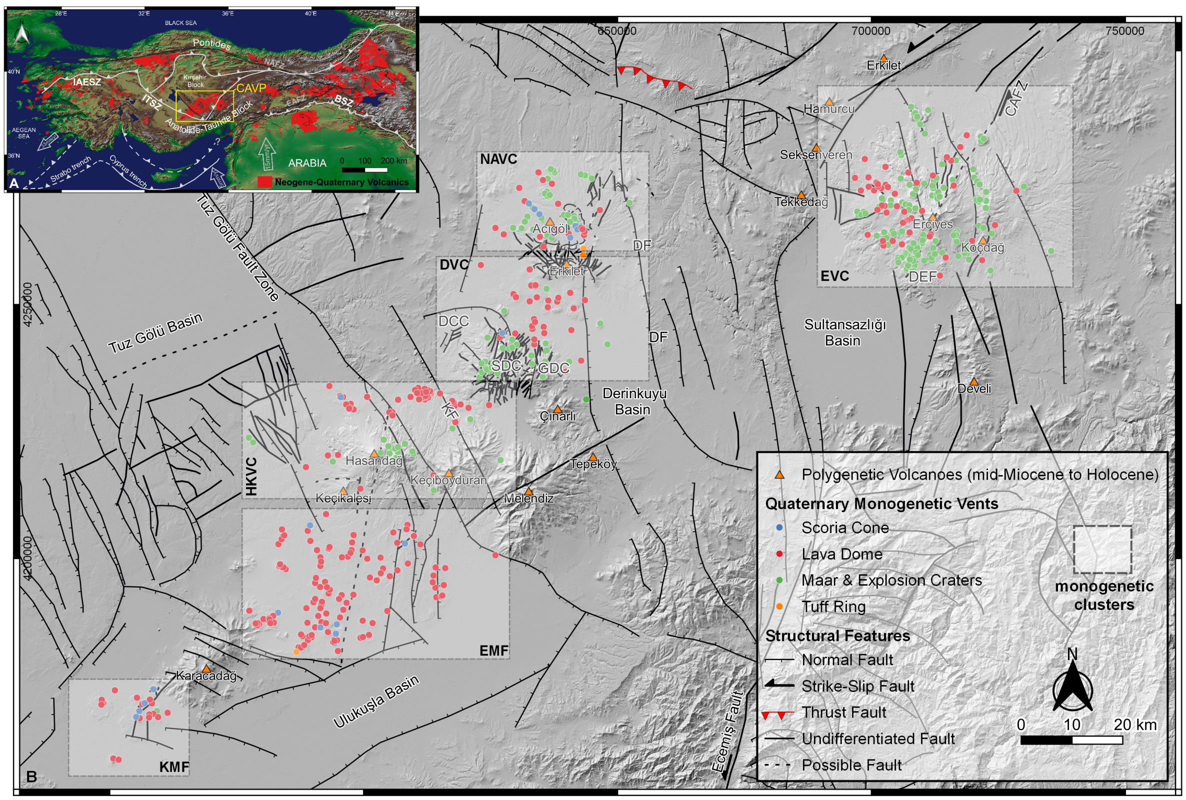

Figure 1: **A.** Inset map showing the Neogene-Quaternary volcanics in the Anatolia (compiled from MTA 1/500000 scale geological maps) and the geographic location of the CAVP (modified after Uslular and Gençalioğlu-Kuşcu, 2019a and references therein); **B.** Distribution of Quaternary monogenetic vents in the CAVP (modified after Toprak, 1998; Arcasoy et al., 2004) displayed on a shaded digital elevation model (ALOS 3D World, 30 m x 30 m resolution). Fault dataset (compiled from Pasquare et al., 1988; Toprak and Göncüoglu, 1993; Dhont et al., 1998; Froger et al., 1998; Genç and Yürür, 2010). IAESZ: İzmir-Ankara-Erzincan Suture Zone; ITSZ: Inner-Tauride Suture Zone; BSZ: Bitlis Suture Zone; EAFZ: East Anatolian Fault Zone; NAFZ: North Anatolian Fault Zone; CAFZ: Central Anatolian Fault Zone; DEF: Dündarlı-Erciyes Fault; DF: Derinkuyu Fault; KF: Keçiboyduran Fault; ŞDC: Şahinkalesi Dome Complex; GDC: Göllüdağ Dome Complex

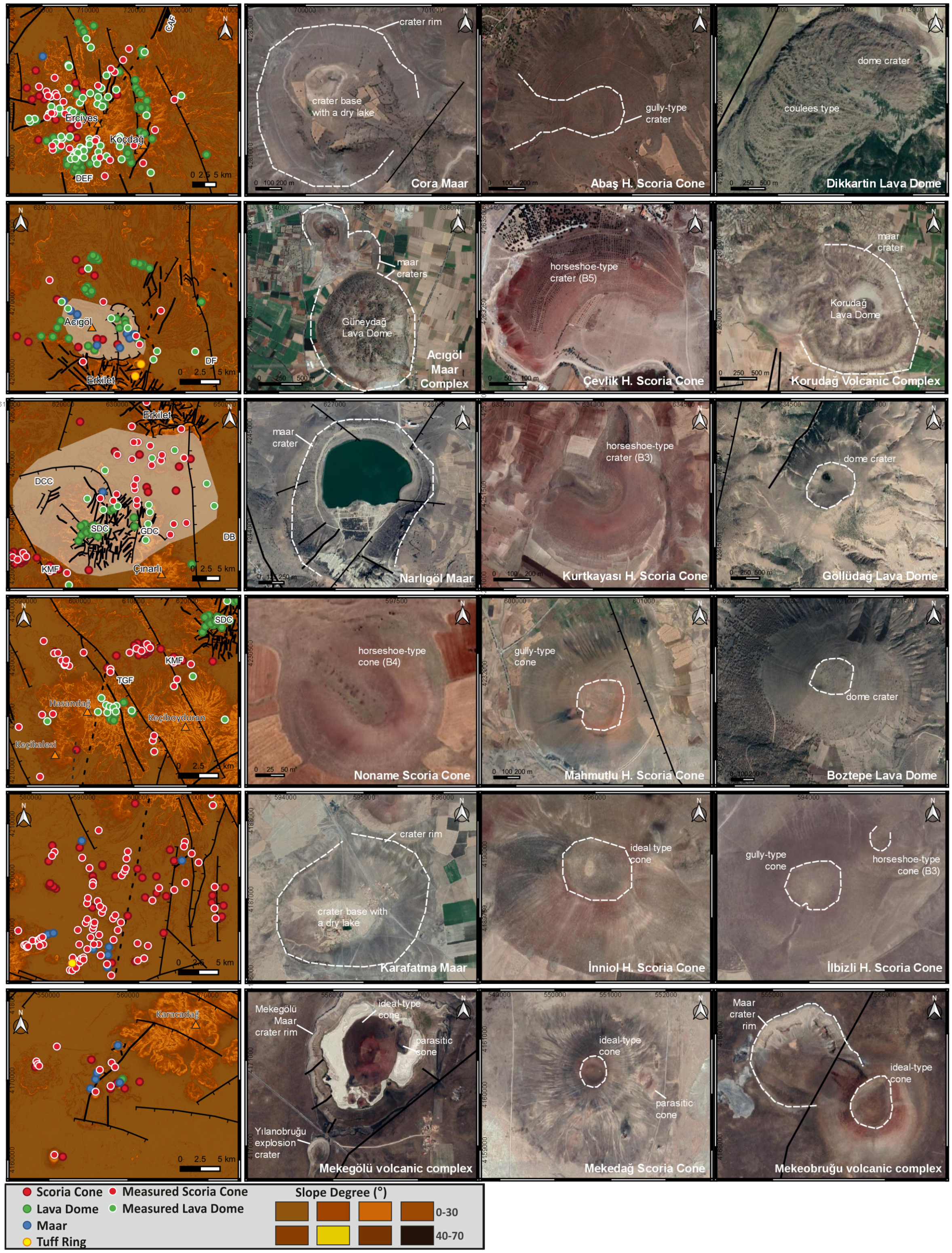

Figure 2: Quaternary monogenetic clusters in the CAVP displayed on the DEM-based (30 m resolution AW3D) slope maps, and Google Earth images of the most representative monogenetic volcanoes from each cluster. References for the fault dataset are as in Fig. 1. Scoria cone morphologies were classified based on (Dóniz-Páez, 2015) and (Bemis and Ferencz, 2017)

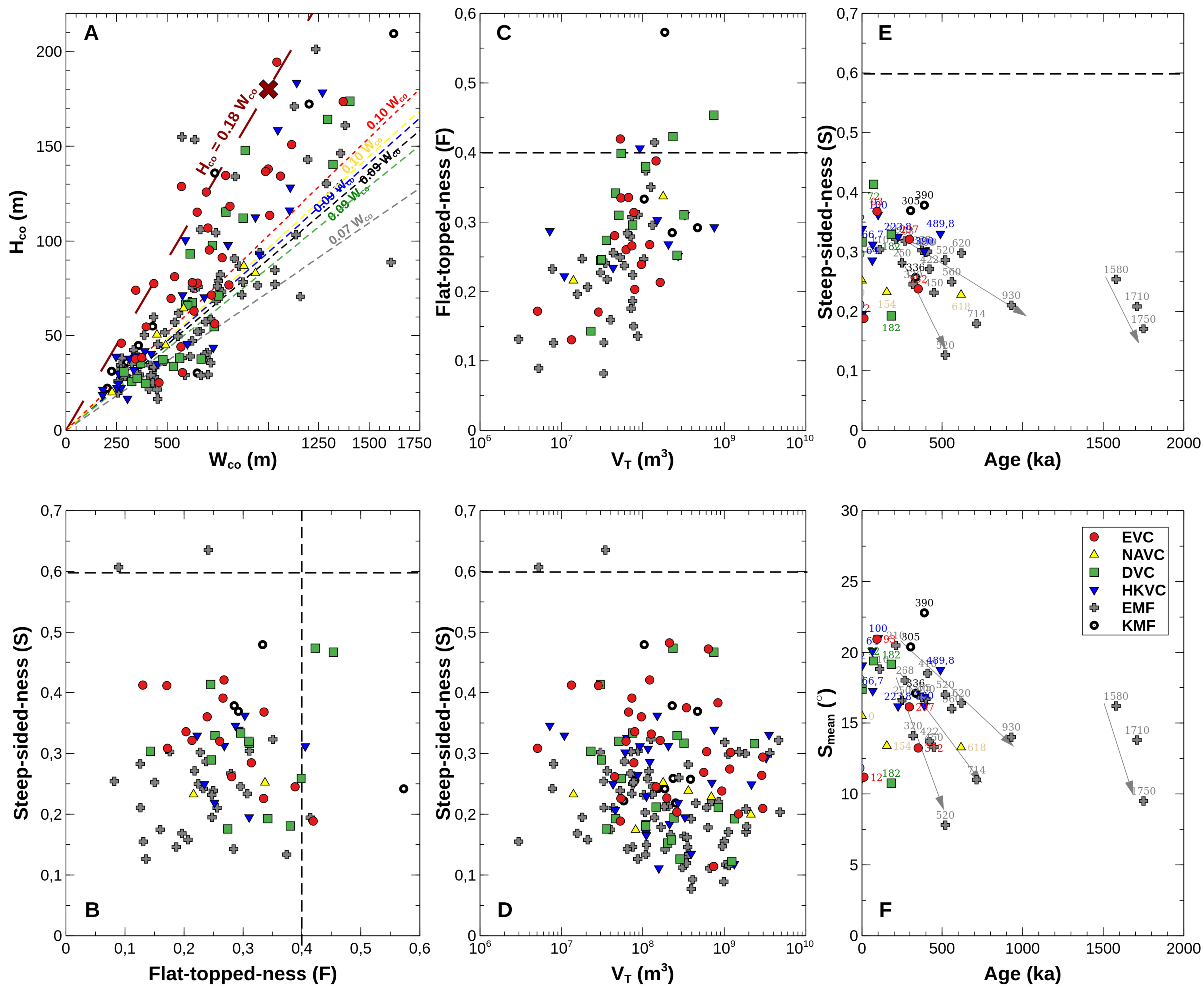

Figure 3: Comparison of morphometric parameters of scoria cones from each monogenetic cluster. Dashed and colored lines in **A** are the regression lines displaying the slope (i.e. ratio) between H_{co} and W_{co}. Dashed lines in **B, C, and D** correspond to the ideal ratios (H_{co}/W_{co} = 0.18; W_{cr}/W_{co} = 0.4; Wood, 1980). The arbitrary arrows in **E, F and G** display the possible decreasing trends in the flank slopes (i.e. steep-sided-ness and S°_{mean}) with regard to increasing cone ages. See text for further details.

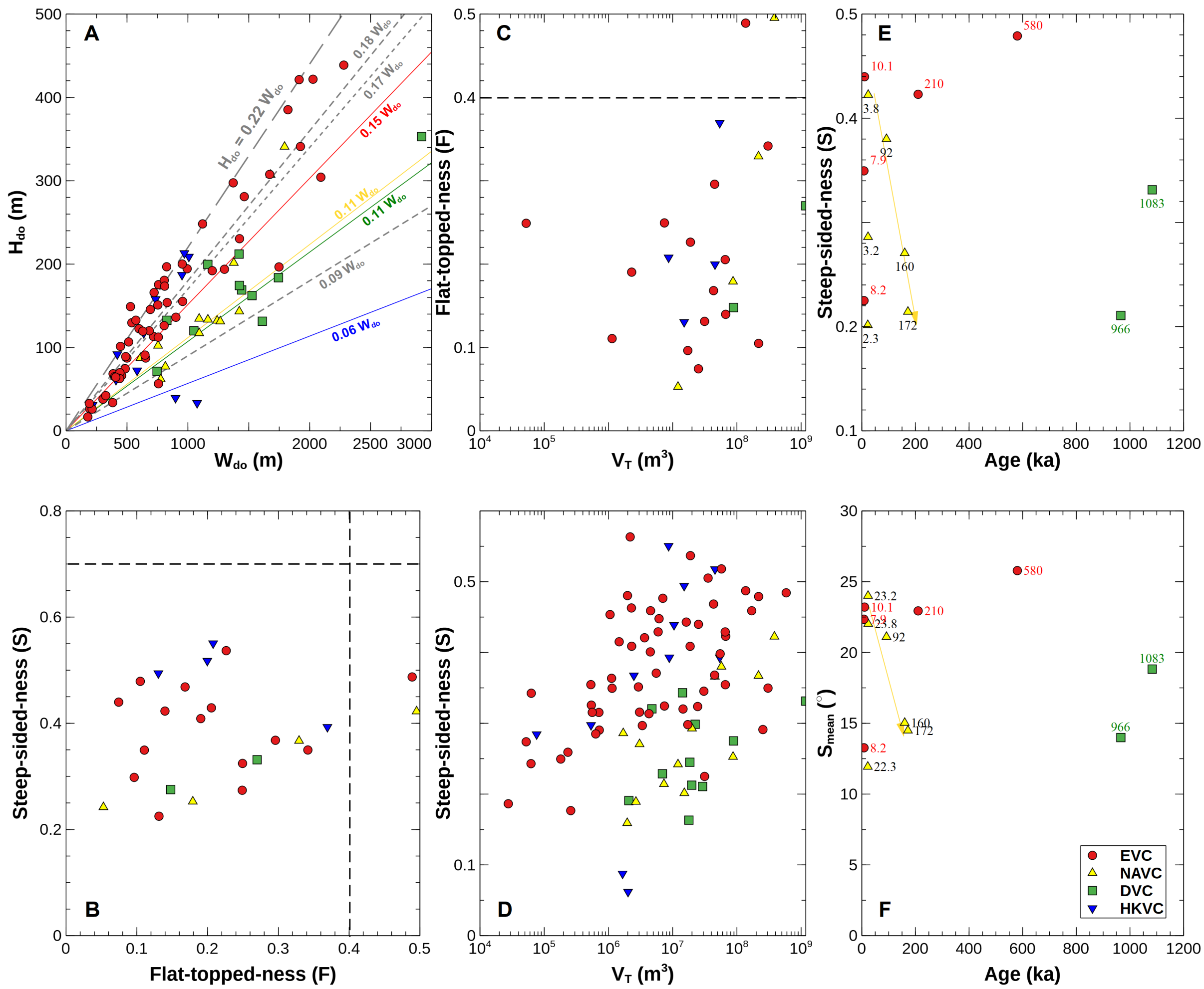

Figure 4: Comparison of morphometric parameters of lava domes from each monogenetic cluster. Gray dashed lines in **A** are the regression lines displaying the ideal slopes (i.e. ratios) between H_{do} and W_{do} based on the different dome morphologies (i.e. general ratio = 0.22; coulèe-type = 0.18; Pelean-type = 0.17; low domes = 0.09; Blake, 1990; Aguirre-Díaz et al., 2006). Dashed lines in **B and C** correspond to the ideal ratios (H_{do}/W_{do} = 0.22 or S = 0.7; Karatson et al., 2013 and references therein; W_{cr}/W_{do} or F = 0.4; after Wood, 1980). The arbitrary yellowish arrows in **E and F** display the possible decreasing trends in the flank slopes (i.e. steep-sided-ness and S°_{mean}) with the increasing dome ages. See text for further details.

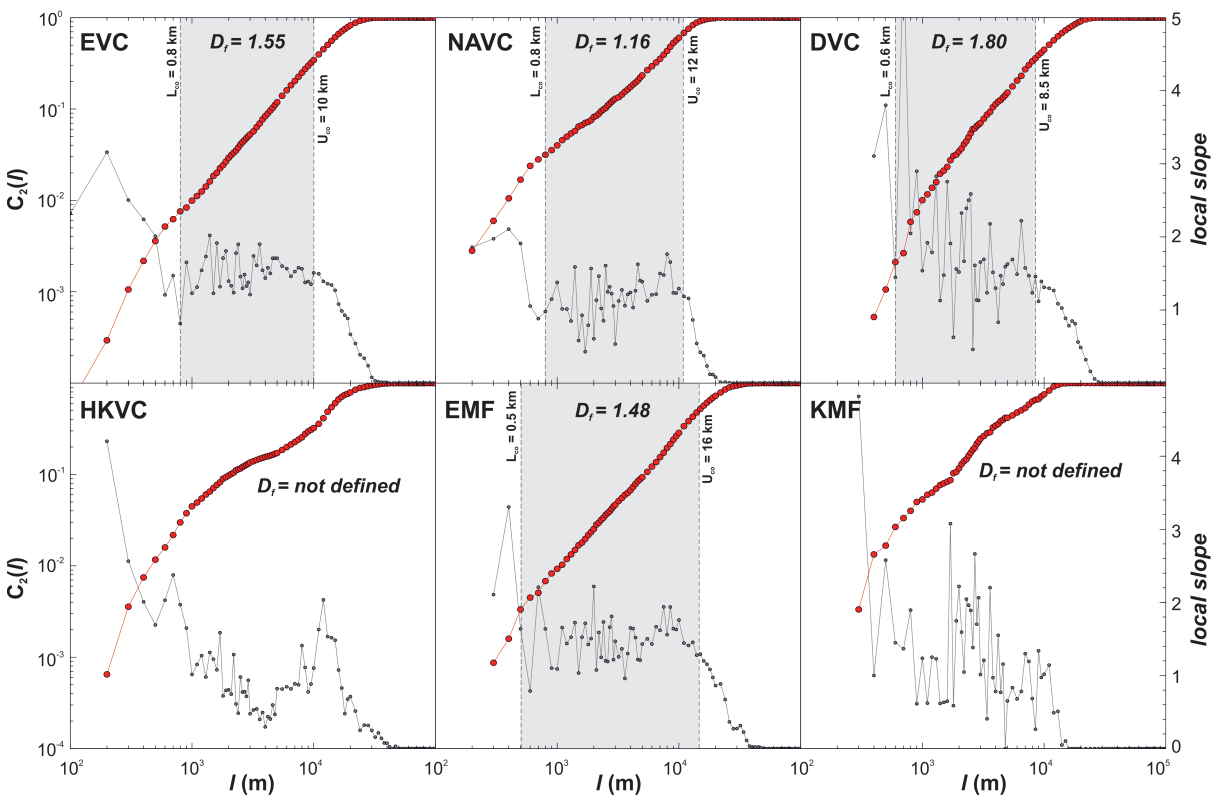

Figure 5: Logarithmic plots of l(m) vs. $C_2(l)$ displaying the fractal (Df) or correlation (D_2) exponents. L_{co}: lower cut-off; U_{co}: upper cut-off

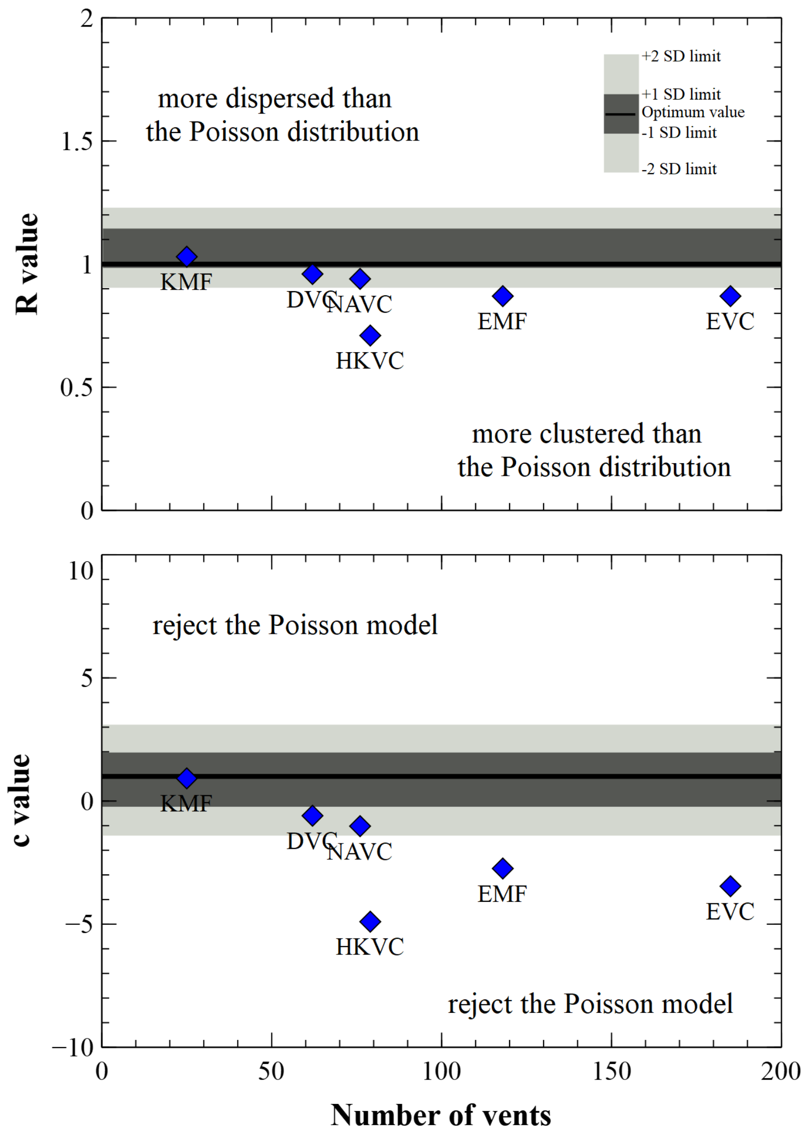

Figure 6: Number of vents in each monogenetic cluster vs. statistical values of R and c plots. Only the DVC fits to Poisson model, but the other MVFs reject the model and display a clustered distribution

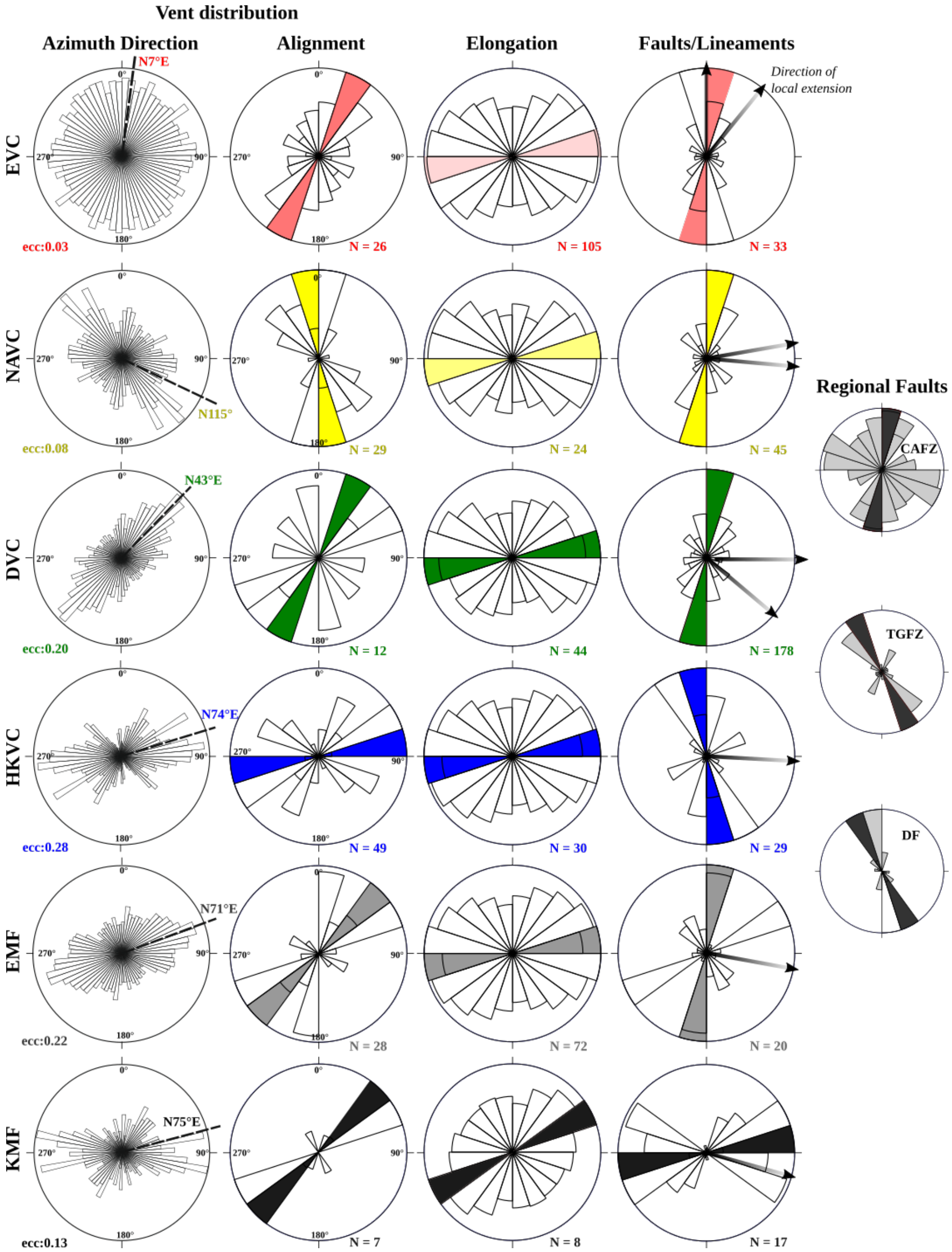

Figure 7: Comparison of azimuth directions and vent alignments with the cone/dome elongations and local and regional fault directions in each monogenetic cluster. Main azimuth trends shown by solid dashed lines were determined by the PCA (i.e. azimuth of the first eigenvector). **N** is the total number of objects (i.e. accepted alignments, cone/dome and faults) used in the analyses. Local extensional axes were adopted from Dhont et al. (1998) and Genç and Yürür (2010)

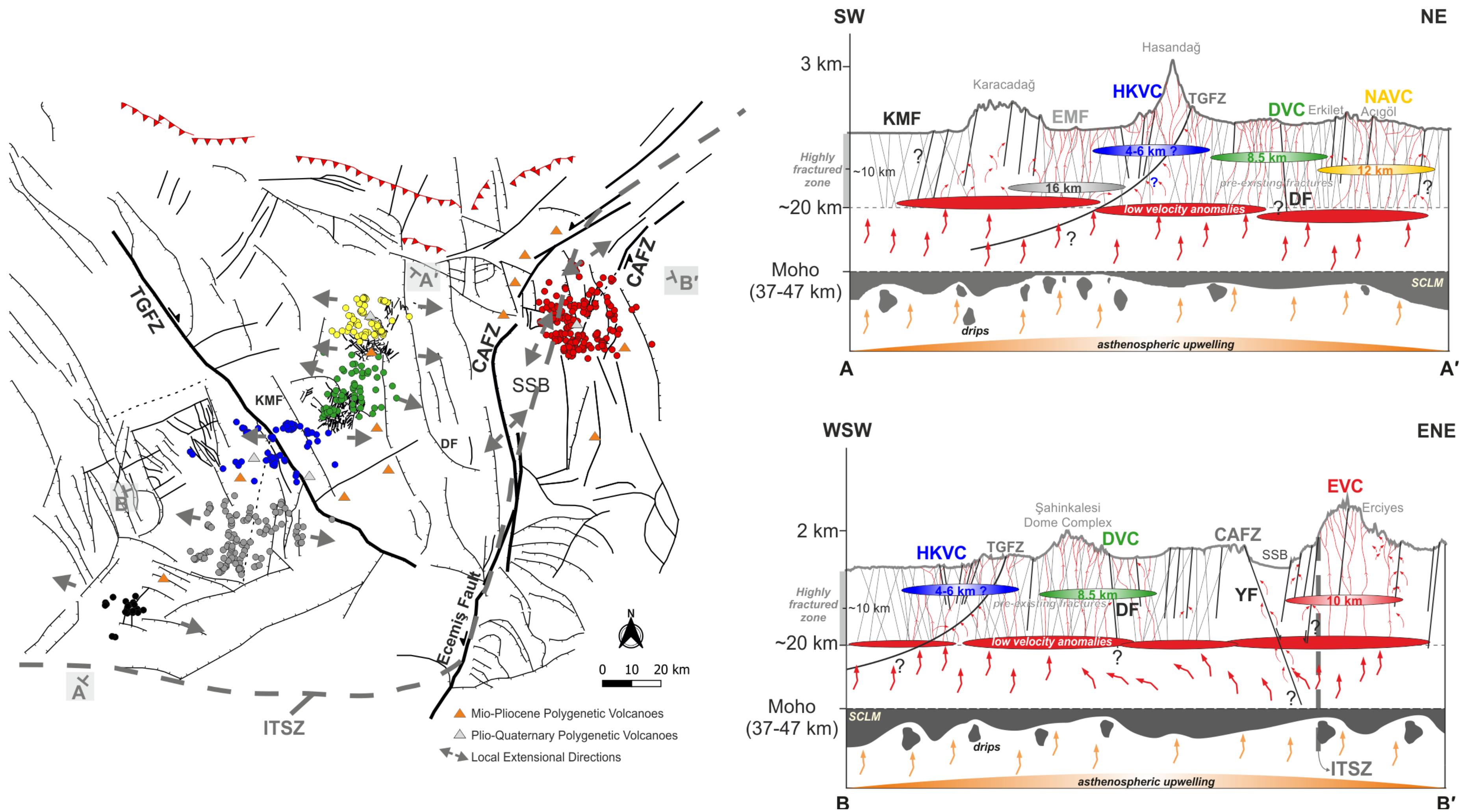

Figure 8: Simplified cross-sections (not to scale) along A-A' and B-B' profiles displaying the main crustal structures beneath the CAVP. The conceptual model for the interaction between upwelling asthenosphere and sub-continental lithospheric mantle (SCLM) was adopted from Reid et al. (2017). See text for further discussions. Possible initial depths of dike intrusions beneath each monogenetic field are inferred from our fractal analysis (i.e. U_{co} values), except for HKVC where the local slope could not be defined (Fig.5), and hence the recent magnetotelluric imaging results (Tank and Karaş, 2020) were adopted. The low-velocity anomalies and possible Moho depth are from Abgarmi et al. (2017) and Vanacore et al. (2013), respectively. Faults illustrated in the CAFZ are those of normal components. The abbreviations on the map are as in Fig.1B.

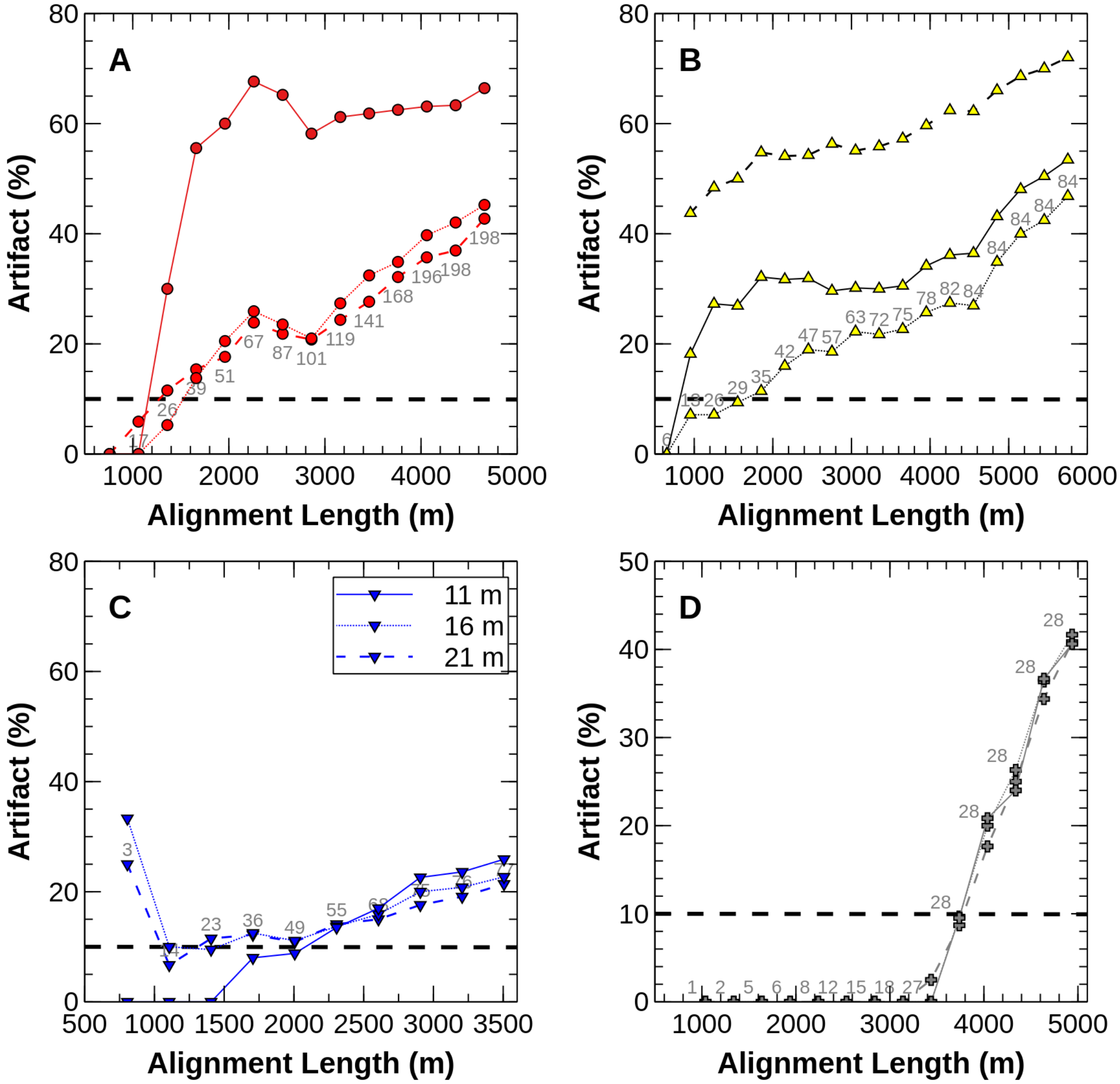

Supplementary Figure SF1. Vent alignment analysis of monogenetic clusters based on the different thicknesses (11, 16 and 22 m). **A.** EVC; **B.** NAVC; **C.** HKVC; and **D.** EMF. The best representative alignment was chosen from those including artifacts ≤10% and higher number of alignment. Styles of lines given as legend in **C** are valid for diagrams with other color coding. All computed alignments in the DVC and KMF were accepted, and hence there is no artifact in these clusters.

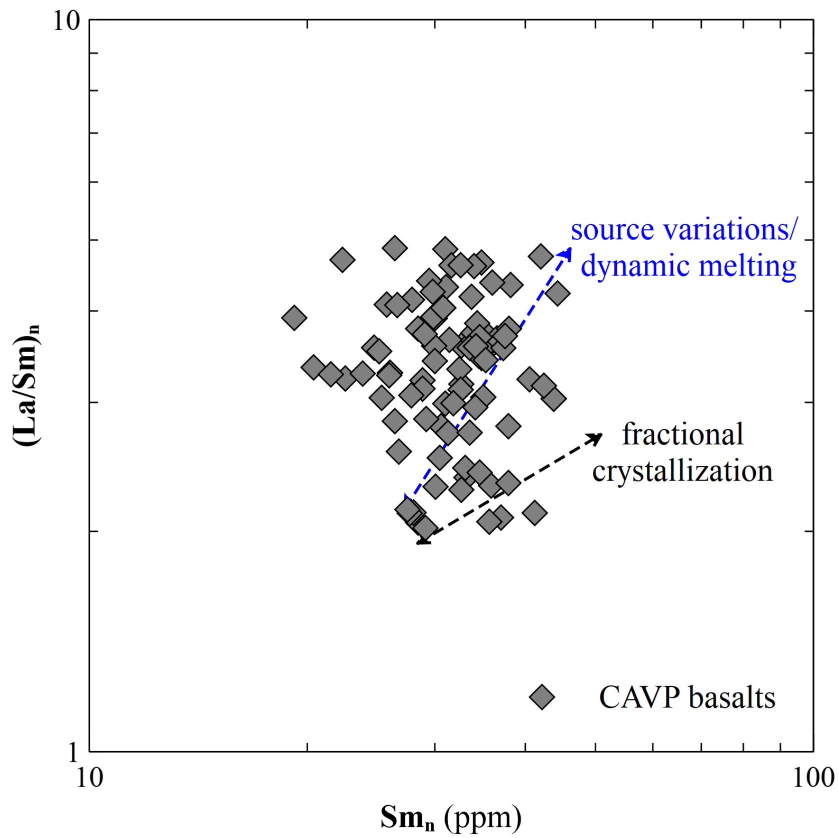

Supplementary Figure SF2. Sm_n (ppm) vs. $(\mathrm{La/Sm})_n$ diagram for the CAVP Quaternary basalts (data from Uslular and Gençalioğlu-Kuşcu, 2019a). Dashed lines were adopted from Pearce et al. (1995)

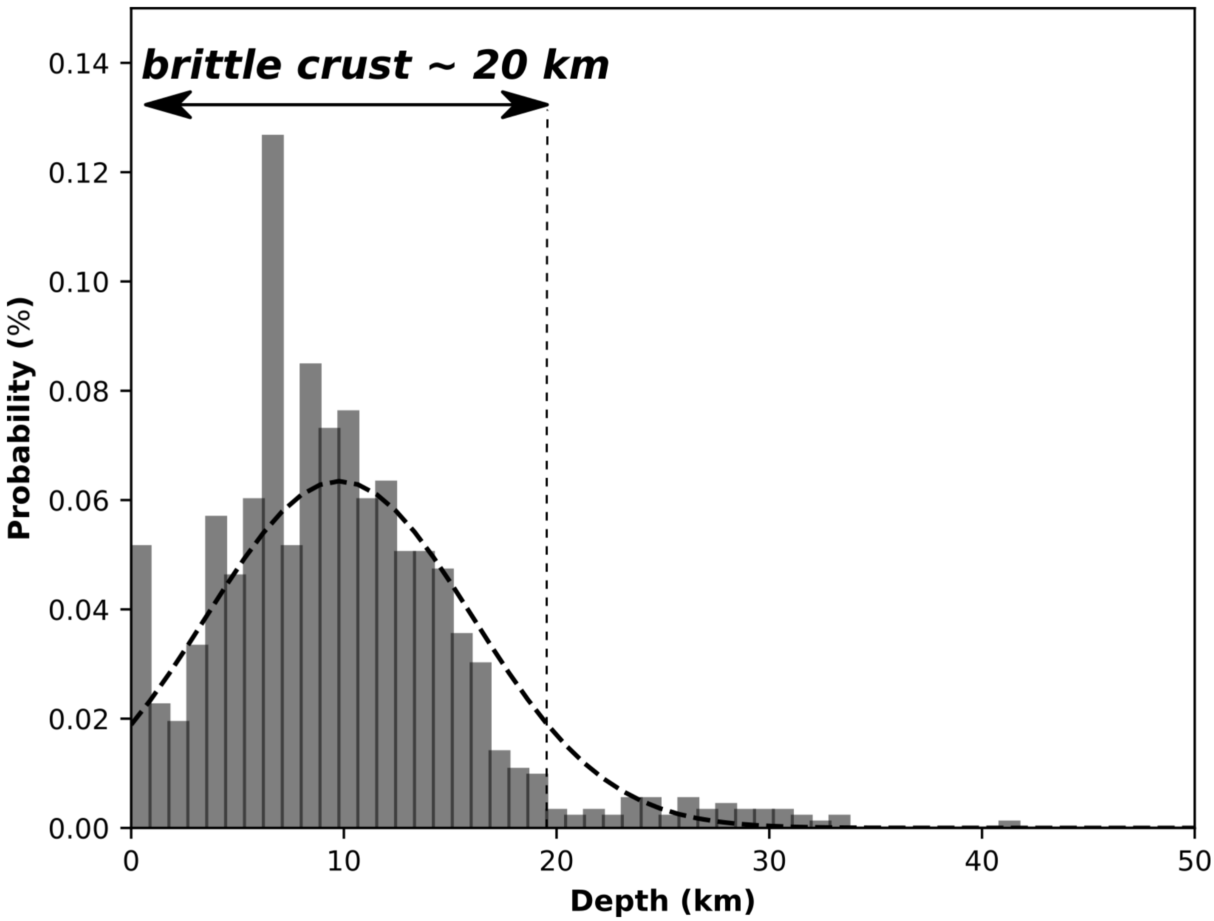

Supplementary Figure SF3. Earthquake dataset for the period of 2010-2019 around central Anatolia (compiled from the catalog of International Seismological Centre), revealing the possible thickness of the seismogenic (or brittle) layer beneath the central Anatolia